iScience

CellPress
OPEN ACCESS

Article

Dissociation of ERMES clusters plays a key role in attenuating the endoplasmic reticulum stress

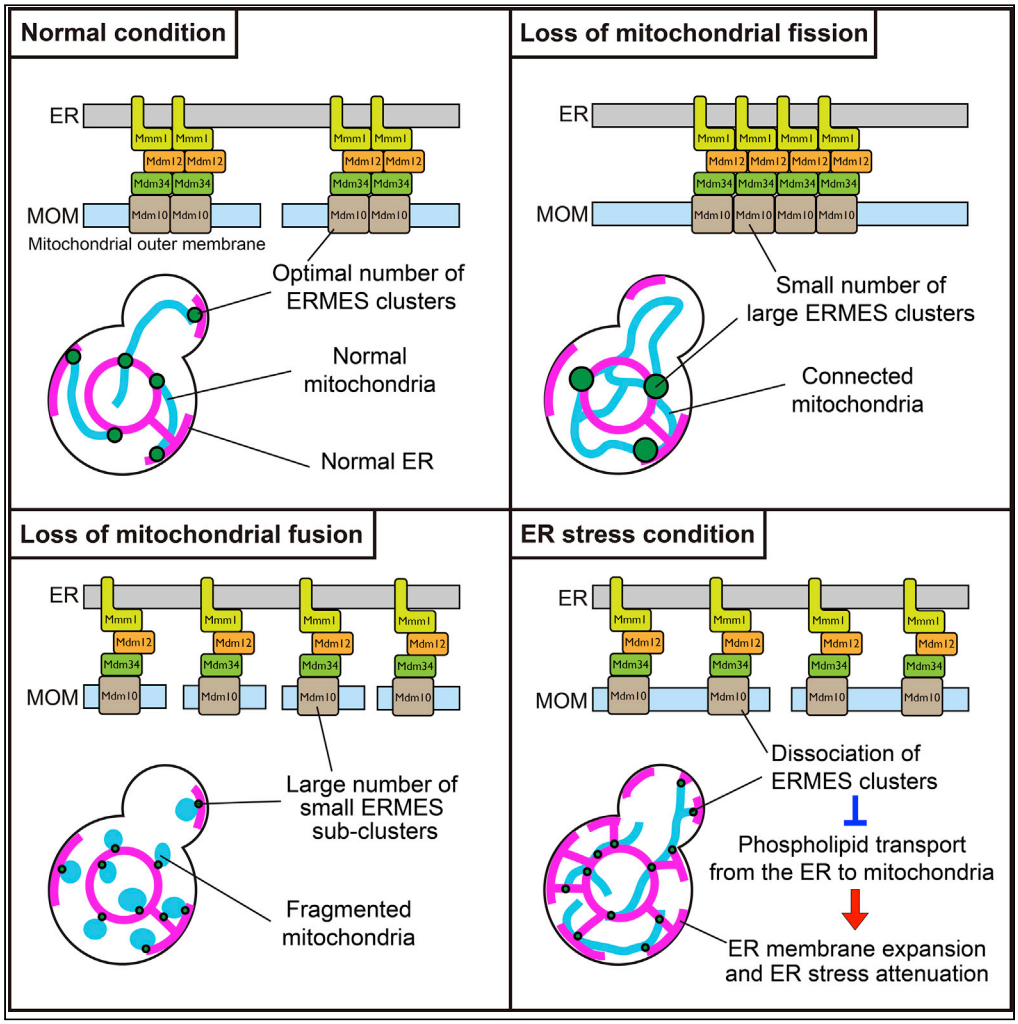

Yuriko Kakimoto-Takeda, Rieko Kojima, Hiroya Shiino, ..., Akihiko Nakano, Toshiya Endo, Yasushi Tamura

tamura@sci.kj.yamagata-u.ac.jp

Highlights

Mitochondrial fusion and division regulate the clustering of the ERMES complex

ER stress leads to dissociation of the ERMES clusters independently of Ire1 and Hac1

The dissociated ERMES complexes have less activity in transporting phospholipids

The defective phospholipid transport may cause the ER expansion to relieve ER stress

Kakimoto-Takeda et al., iScience 25, 105362 November 18, 2022 © 2022 The Authors.
https://doi.org/10.1016/j.isci.2022.105362

iScience

CellPress
OPEN ACCESS

Article

Dissociation of ERMES clusters plays a key role in attenuating the endoplasmic reticulum stress

Yuriko Kakimoto-Takeda,[1,6] Rieko Kojima,[2,6,7] Hiroya Shiino,[2] Manatsu Shinmyo,[2] Kazuo Kurokawa,[3] Akihiko Nakano,[3] Toshiya Endo,[4,5] and Yasushi Tamura[2,8,*]

SUMMARY

In yeast, ERMES, which mediates phospholipid transport between the ER and mitochondria, forms a limited number of oligomeric clusters at ER-mitochondria contact sites in a cell. Although the number of the ERMES clusters appears to be regulated to maintain proper inter-organelle phospholipid trafficking, its underlying mechanism and physiological relevance remain poorly understood. Here, we show that mitochondrial dynamics control the number of ERMES clusters. Moreover, we find that ER stress causes dissociation of the ERMES clusters independently of Ire1 and Hac1, canonical ER-stress response pathway components, leading to a delay in the phospholipid transport from the ER to mitochondria. Our biochemical and genetic analyses strongly suggest that the impaired phospholipid transport contributes to phospholipid accumulation in the ER, expanding the ER for ER stress attenuation. We thus propose that the ERMES dissociation constitutes an overlooked pathway of the ER stress response that operates in addition to the canonical Ire1/Hac1-dependent pathway.

INTRODUCTION

In eukaryotic cells, highly developed organelle membranes exert specialized functions that are critical for versatile and vital activities in cells. The sizes and shapes of the organelle membranes are properly regulated and can dynamically respond to the changes in nutrient or stress conditions. For instance, in budding yeast, the volume of mitochondria is kept relatively small under fermentation conditions, whereas it increases drastically on a shift to non-fermentation conditions where the mitochondrial respiratory capacity is critical (Di Bartolomeo et al., 2020). Another example is the endoplasmic reticulum (ER) membrane, which is known to significantly expand on ER stress to alleviate the stress (Schuck et al., 2009). These well-known examples point to the importance of the dynamic remodeling of the organelle membranes, leading to the changes in the amounts of organelle membranes, in the cellular adaptation to the environments. It is then natural to assume that such changes in the amounts of organelle membranes are associated with the regulation of the amounts of resident molecules in each organelle membrane. Because phospholipids are the major constituents of organelle membranes, their synthesis and/or transport should be a key to control the organelle volumes.

Most phospholipids are synthesized in the ER and then transported to various organelle membranes, including mitochondria (Carman and Han, 2011; Dimmer and Rapaport, 2017; Tamura et al., 2019a; Tatsuta and Langer, 2017). Phospholipid transport between the ER and mitochondria is known to be mediated by the ER-mitochondria encounter structure (ERMES) in yeast, which also functions as the molecular tether between these organelles (Jeong et al., 2016,2017; Kawano et al., 2018; Kojima et al., 2016; Kornmann et al., 2009). The ERMES complex consists of four core subunits, ER-resident Mmm1, mitochondrial outer membrane (MOM)-resident Mdm10 and Mdm34, and a peripheral membrane protein Mdm12, although Mdm10 shuttles between ERMES and the machinery for the β-barrel protein assembly, the SAM/TOB complex (Eisenberg-Bord et al., 2016; Lang et al., 2015; Murley and Nunnari, 2016; Tamura and Endo, 2017). ERMES forms large oligomeric clusters that can be observed as several discrete foci in cells by fluorescence microscopy when an ERMES subunit is expressed as a fusion protein with a fluorescent protein (Berger et al., 1997; Burgess et al., 1994; Dimmer et al., 2002; Sogo and Yaffe, 1994). We hereafter call ERMES clusters as ERMES dots. The number of discrete ERMES dots in a cell appears to be regulated depending on the

[1]Department of Biochemistry and Molecular Biology, Graduate School of Medical Science, Yamagata University, 2-2-2 Iidanishi, Yamagata 990-9585, Japan

[2]Faculty of Science, Yamagata University, 1-4-12 Kojirakawa-machi, Yamagata 990-8560, Japan

[3]Live Cell Super-Resolution Imaging Research Team, RIKEN Center for Advanced Photonics, 2-1 Hirosawa, Wako, Saitama 351-0198, Japan

[4]Faculty of Life Sciences, Kyoto Sangyo University, Kamigamo-motoyama, Kita-ku, Kyoto 603-8555, Japan

[5]Institute for Protein Dynamics, Kyoto Sangyo University, Kamigamo-motoyama, Kita-ku, Kyoto 603-8555, Japan

[6]These authors contributed equally

[7]Present address: Toyama Prefectural Institute for Pharmaceutical Research, 17-1 Nakataikouyama, Imizu, Toyama 939-0363, Japan

[8]Lead contact

*Correspondence: tamura@sci.kj.yamagata-u.ac.jp

https://doi.org/10.1016/j.isci.2022.105362

This is an open access article under the CC BY-NC-ND license (http://creativecommons.org/licenses/by-nc-nd/4.0/).

environments. For example, the number of ERMES dots increases with a change in the metabolic state, such as a shift from the fermentation to non-fermentation culturing condition, which promotes mitochondrial proliferation (Hönscher et al., 2014). Physical association of mitochondria with the vacuole, termed vCLAMP (vacuole and mitochondria patch), exhibits a behavior opposite to ERMES with regard to the degree of membrane contacts; under non-fermentable conditions, Vps39, which is responsible for the formation of vCLAMP, is phosphorylated, resulting in a decreased number of vCLAMP (Hönscher et al., 2014). These observations suggest that mitochondria-ER contacts and mitochondria-vacuole contacts mediated by ERMES and Vps39, respectively, are reciprocally regulated and that the functions of ERMES and vCLAMP partly overlap (Elbaz-Alon et al., 2014; Hönscher et al., 2014). A high-content imaging screen for yeast deletion mutants with an altered number of ERMES dots revealed that the loss of Vps39 or mitochondrial division factors, such as Dnm1 and Fis1, leads to an increased number of ERMES dots (Elbaz-Alon et al., 2014). These observations also suggest the presence of the regulatory mechanism of the number and degree of the inter-organelle contacts. Nevertheless, the mechanisms underlying regulation of the dynamics of the inter-organelle contacts are largely unknown.

We attempted here to characterize the dynamics of ERMES dots by searching for the factors that affect the number or degree of the ERMES dots. We found that mitochondrial morphological dynamics such as division and fusion of mitochondria affected the number of ERMES dots in a cell. Analysis of the mitochondrial division and fusion-dependent changes revealed that ERMES dots undergo association of and dissociation into smaller ERMES sub-clusters. The dissociation of large ERMES dots was also promoted by ER stress, although this response is independent of Ire1 and Hac1, which constitute canonical ER stress response pathway. Of importance, we found that the phospholipid transport from the ER to mitochondria slowed down on the ERMES dissociation. Besides, we noticed that ER membrane expansion induced by the ER stress was suppressed in *mmm1-1* cells which were defective in the dissociation of ERMES dots. On the basis of these findings, we will forward a model that dissociation of the ERMES dots acts as a brake to prevent the phospholipid leakage from the ER, thereby contributing to the ER membrane expansion, which may be crucial for attenuation of the ER stress.

RESULTS

Mitochondrial fusion and division antagonistically affect the number of ERMES dots

To characterize the dynamic behaviors of the mitochondria-ER contact sites, we first looked for the factors that would affect the number of the contact sites. To search for such factors, we visualized the mitochondria-ER contact sites with the split-GFP probes (Kakimoto et al., 2018; Tashiro et al., 2020) in yeast cells that lacked or downregulated each of the 53, reported MOM proteins (see STAR methods). The number of visualized mitochondria-ER contact sites clearly decreased in the strain lacking Fis1, which functions as a receptor for the mitochondrial division factor Dnm1 (Figure S1A)(Bleazard et al., 1999; Mozdy et al., 2000). This observation is not consistent with the previous report that the number of ERMES dots, as observed by tagging of a fluorescent protein to the ERMES subunit, increased in the absence of Dnm1 or Fis1 (Elbaz-Alon et al., 2014). Therefore, we further asked if the loss of the mitochondrial division would affect the appearance of the mitochondria-ER contact sites. We observed ERMES dots in wild-type, *dnm1Δ*, and *fis1Δ* cells expressing mitochondria-targeted red fluorescent protein (RFP) (Su9-RFP) and C-terminally green fluorescent protein (GFP)-tagged Mmm1 (Mmm1-GFP) by confocal fluorescence microscopy. We acquired approximately 5-μm thick z stack images, incrementally spaced by 0.2 μm that covered an entire cell (Figure 1A). To minimize the undesired effects on the appearance of ERMES dots such as those arising from possible variations of the Mmm1-GFP expression level, we adopted stable expression of Mmm1-GFP from the chromosome. Maximum projection images reconstituted from the z-stacks showed that ERMES dots were localized on mitochondrial tubules in wild-type, *dnm1*Δ, and *fis1*Δ cells, although the mitochondrial distribution was altered because of the lack of the mitochondrial division in *dnm1*Δ and *fis1*Δ cells. The wild-type, *dnm1*Δ, and *fis1*Δ cells contained an average of 5.8, 3.5, and 3.0 ERMES dots per cell, respectively (Figure 1B). These results indicate that loss of mitochondrial division leads to a decrease in the number of ERMES dots. The reduced ERMES number observed in mitochondrial division-deficient cells was not because of decreased levels of ERMES subunits because the amounts of Mmm1, Mdm12, and Mdm34 were all comparable between *dnm1*Δ and wild-type cells (Figure S1B).

We then re-examined the previously reported effects of the loss of vCLAMP components on the number of ERMES foci. Although the vCLAMP component Vps39 was found as a factor whose absence led to an increase in the number of ERMES dots (Elbaz-Alon et al., 2014), we did not observe a drastic change in

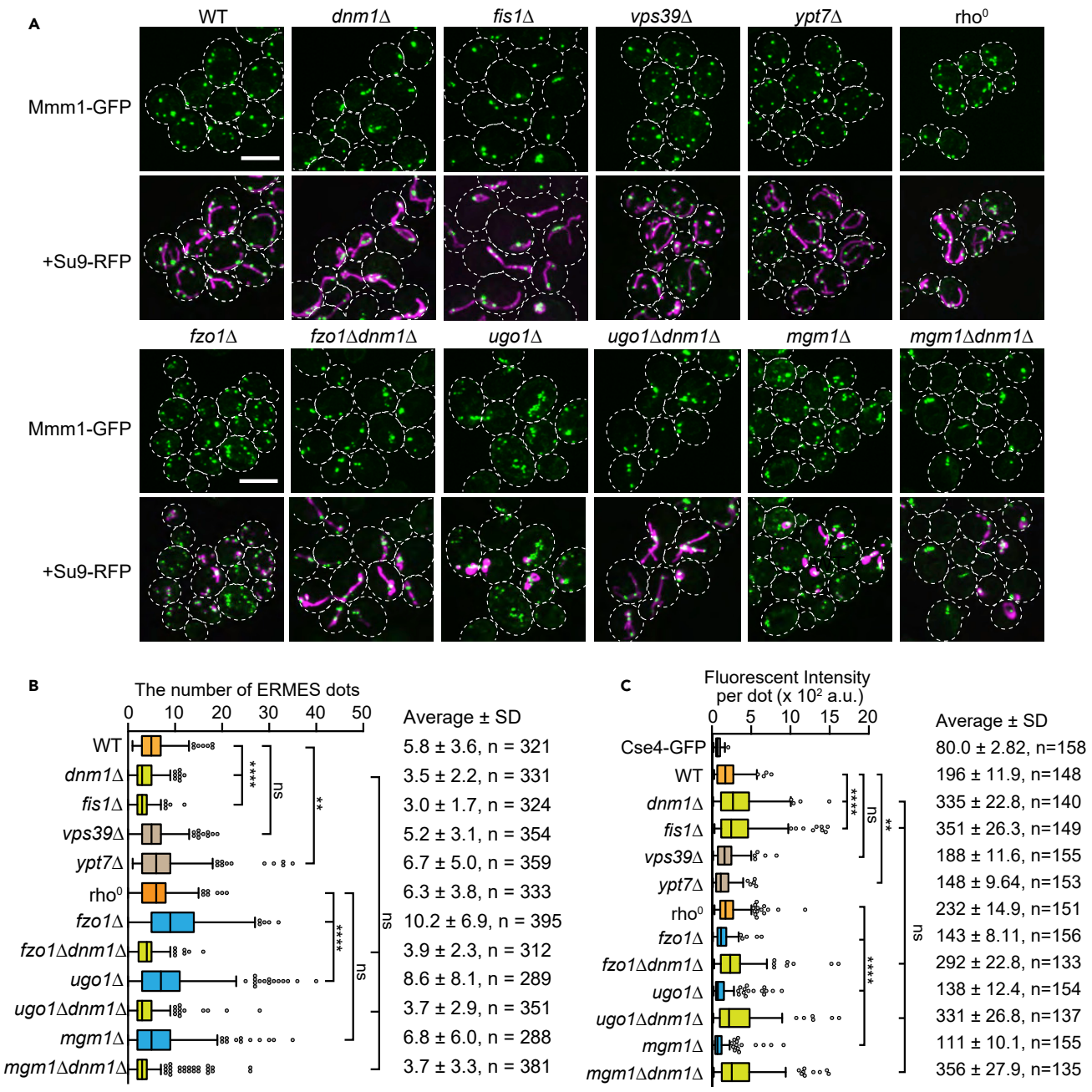

Figure 1. Mitochondrial fusion and division antagonistically regulate the number of ERMES dots

(A) The indicated yeast cells expressing Mmm1-GFP and mitochondria-targeted RFP (Su9-RFP) were imaged under a confocal fluorescence microscope. Maximum projection images were shown. Scale bars, 5 μm.

(B) Box and whisker plots show the distribution of the number of ERMES dots per cell. SD means standard deviation. **: p< 0.001,****: p< 0.0001, p values were obtained from the unpaired two-tailed t-test with Welch's correction.

(C) Quantifications of signal intensities of ERMES dots in the indicated cells using Cse4-GFP signal as a standard. Box and whisker plots show the estimated number of Mmm1-GFP molecules included in a single ERMES dot. The average intensity of Cse4-GFP foci was set to 80 U. ns: not significant, **: p< 0.001,****: p< 0.0001, p values were obtained from the unpaired two-tailed t-test with Welch's correction.

the number of ERMES dots in *vps39*Δ cells as compared with that of wild-type cells (Figures 1A and 1B). On the other hand, loss of another vCLAMP component Ypt7 led to a slight increase in the ERMES dot number. These results collectively suggest that factors other than vCLAMP, e.g., the growth phase, growth media,

yeast strain backgrounds, or performance of microscope, could also affect the appearance of ERMES dots in a complex manner.

We next tried to directly assess the number of Mmm1-GFP molecules contained in a single ERMES dot from their GFP signals using Cse4-GFP, which is a centromeric histone H3-like protein (Figure S1C). Because it is known that Cse4-GFP forms a kinetochore cluster that contains ~80 molecules of Cse4-GFP, we used the Cse4-GFP dot as a reference to quantify the number of GFP molecules in a single ERMES dot (Coffman et al., 2011; Joglekar et al., 2006; Lawrimore et al., 2011; Yamamoto et al., 2012). Of interest, each of the clustered ERMES dots in *dnm1*Δ and *fis1*Δ cells contained an average of 335 and 351 of Mmm1-GFP molecules, respectively, which were significantly larger than 196 molecules per dot observed in wild-type cells (Figure 1C). The average numbers of Mmm1-GFP molecules per ERMES dot were similar in *vps39*Δ and slightly smaller in *ypt7*Δ cells as compared with that in wild-type cells. These results suggest that the reduced number of ERMES dots in yeast mutant cells defective in mitochondrial division reflects enhanced clustering of the preexisting ERMES dots. Thus, proper mitochondrial division may inhibit unnecessary aggregation of ERMES dots, thereby maintaining the optimum number of the ERMES dots in a cell.

If mitochondrial division suppresses clustering of the preexisting ERMES dots and thereby controls the optimum number of ERMES dots, inhibition of the mitochondrial fusion will, in turn, increase the number of ERMES dots due to ongoing mitochondrial division. We thus deleted the mitochondrial fusion genes, *FZO1*, *UGO1*, or *MGM1* (Hermann et al., 1998; Sesaki and Jensen, 2001; Wong et al., 2000), and observed the ERMES dots visualized with Mmm1-GFP. Since the lack of mitochondrial fusion could cause loss of mtDNA, we used a *rho*^{0} strain lacking the mtDNA as a control to simplify the interpretation. Supporting our reasoning, defects in the mitochondrial fusion by deletion of the *FZO1* and *UGO1* genes for the mitochondrial outer membrane (MOM) fusion increased the number of ERMES dots, while the loss of mtDNA alone did not (Figures 1A and 1B). Although we detected ERMES dots that were not colocalized with a mitochondrial matrix marker, Su9-RFP especially in *ugo1*Δ cells (Figure 1A), we confirmed that all the ERMES dots were co-stained with a MOM marker Tom71-mCherry (Figure S1D). Indeed, we observed that the fluorescence signals arising from Tom71-mCheery and Su9-BFP were not completely overlapped in *ugo1*Δ cells (Figure S1D), suggesting that there are a lot of mitochondria that can be stained efficiently with Tom71-mCherry but not with Su9-BFP in *ugo1*Δ cells. We thus conclude that all the ERMES dots represent the ER-mitochondria contact sites. Deletion of the mitochondrial inner membrane (MIM) fusion gene, *MGM1*, caused an increase in the number of the cells that contained >10 ERMES dots, which were rarely observed for wild-type cells although the average ERMES dot number was not significantly increased in *mgm1Δ* cells. This result suggests that Mgm1-mediated MIM fusion is not entirely coupled with the Fzo1-mediated MOM fusion (Meeusen et al., 2004). Further supporting the role of the mitochondrial division in controlling the number of ERMES dots, loss of the division gene *DNM1* together with the loss of a fusion gene, *FZO1*, *UGO1*, or *MGM1* reversed the above phenotypes. That is, although *fzo1Δdnm1Δ* and *ugo1Δdnm1Δ* cells exhibited tubular mitochondria because of simultaneous defects in mitochondrial fusion and division as reported (Sesaki and Jensen, 1999), the number of ERMES dots was altered to such a level that is similar to the number in *dnm1Δ* cells, regardless of the simultaneous deletion of *FZO1* or *UGO1* (Figures 1A and 1B). Besides, when mitochondrial fusion was inhibited, the estimated number of Mmm1-GFP molecules per ERMES dot was smaller than those in wild-type and *rho*^{0} cells. On the other hand, when *DNM1* was deleted together with *FZO1*, *UGO1* or *MGM1*, the number of Mmm1-GFP molecules per ERMES dot was drastically increased to the level similar to *dnm1*Δ cells (Figure 1C). These results suggest that the mitochondrial fusion and division can antagonistically affect the number of ERMES dots by controlling the clustering of preexisting ERMES dots.

Preexisting ERMES dots cluster together

To test the idea that the preexisting ERMES dots gather together, we utilized a yeast mating assay to monitor the mitochondrial fusion directly (Sesaki et al., 2003) (Figure 2A). Briefly, we constructed two types of yeast cells with opposing mating types (MATa and MATα) that expressed Mmm1-GFP or Mmm1-mScarlet under the control of the *GAL1* promoter. We then examined how the ERMES dots behaved after cell fusion. If preexisting ERMES dots tend to cluster together, the green- and red-labeled dots should become merged or adjacent to each other after cell fusion (Figure 2A). To exclude the possibility that Mmm1-GFP molecules newly synthesized after cell fusion congregate into preexisting ERMES dots containing Mmm1-mScarlet, or vice versa, we suppressed the expression of both Mmm1-GFP and Mmm1-mScarlet before mating by cultivating the cells in a glucose-containing medium YPD for 4 h.

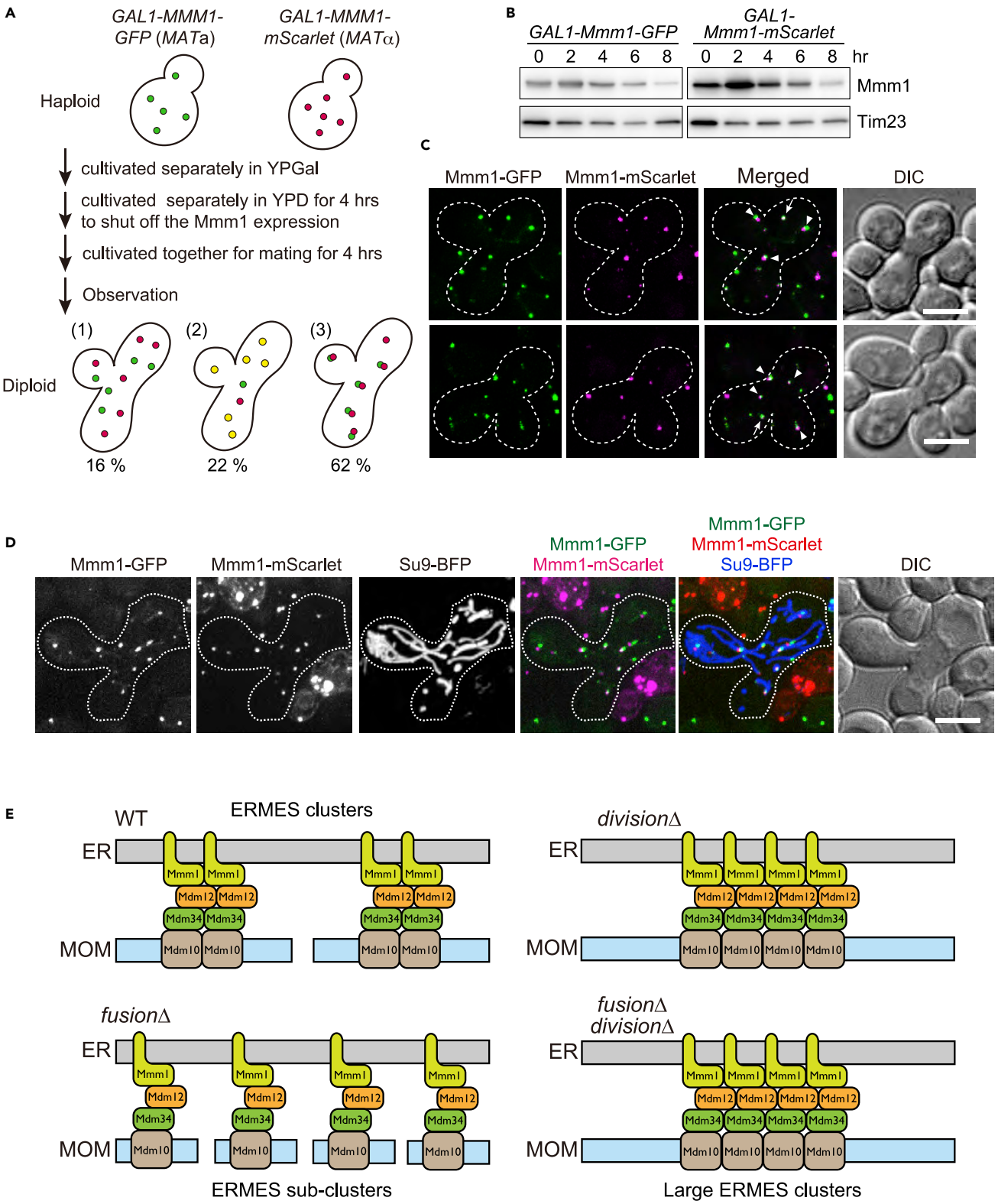

Figure 2. Preexisting ERMES dots cluster together on cell fusion

(A) A schematic diagram of the mating assay showing possible patterns of the ERMES dots. (1) The preexisting ERMES foci do not cluster together. (2, 3) The preexisting ERMES foci merge completely (2) or contact each other (3).

Figure 2. *Continued*

(B) Whole cell extracts prepared from yeast cells after shutting off the expression of Mmm1-GFP or Mmm1-mScarlet were subjected to immunoblotting using antibodies against Mmm1 and Tim23.

(C) Yeast zygotes obtained by mating haploid cells containing ERMES dots labeled with different fluorescent colors. Scale bars, 5 μm. Arrowheads and arrows indicate adjacent and merged ERMES dots, respectively.

(D) Yeast zygotes expressing Mmm1-GFP, Mmm1-mScarlet, and Su9-BFP. Scale bars, 5 μm.

(E) A working model for regulating the number of ERMES dots by mitochondrial fusion and division.

Immunoblotting of whole cell lysates confirmed that Mmm1-GFP and Mmm1-mScarlet were depleted after 4 h cultivation in YPD (Figure 2B). Strikingly, most zygotes contained ERMES dots labeled with different fluorescent proteins that were adjacent to each other (62%) or completely merged (22%) (Figures 2A and 2C). We confirmed that the adjacent ERMES dots were present on the same mitochondria (Figure 2D). These observations suggest that the different preexisting ERMES dots or "sub-clusters" contact with each other to form large clusters, although the sub-clusters may not completely fuse or mixed with each other. This supports again the above idea that the proper balance of mitochondrial fusion and division may well regulate the clustering of preexisting ERMES sub-clusters, thereby maintaining a constant number of large ERMES dots (Figure 2E).

The ERMES dot number increases on ER stress in an Ire1-and Hac1-independent manner

Do the association and dissociation of ERMES sub-clusters have any physiological significance? Considering the role of the ERMES complex in the phospholipid transport between the ER and mitochondria, we reasoned that ER stress, which causes the ER membrane expansion would be a key event to answer this question. Specifically, we hypothesized that the lipid transport function of ERMES may be modulated to accumulate phospholipids in the ER to enlarge the ER membrane. We thus asked if ER stress would affect the number of ERMES dots to deal with the stress. We treated yeast cells expressing Mmm1-GFP with tunicamycin or DTT for 2 h to induce ER stress and determined the ERMES dot numbers using fluorescence microscopy. Strikingly, the number of ERMES dots increased approximately two-fold on treatment of the cells with tunicamycin or DTT (Figures 3A and 3B). This increase in the ERMES dot number on ER stress was not because of the accelerated mitochondrial fragmentation, because the tunicamycin or DTT treatment increased the number of ERMES dots even in the absence of a division factor Dnm1 (Figures 3A and 3B).

We next explored whether the increase in the number of ERMES dots would depend on the canonical unfolded protein response (UPR) (Walter and Ron, 2011). In yeast, an ER-resident type I TM protein Ire1 senses accumulation of aberrant proteins in the ER, and then Ire1 undergoes self-oligomerization, which triggers its kinase and endonuclease activation, leading to Ire1-mediated *HAC1* mRNA splicing (Korennykh et al., 2009). The spliced mature *HAC1* mRNAs produce the functional form of the Hac1 transcription factor, which activates a number of genes that are repressed under non-stress conditions (Kawahara et al., 1997; Sidrauski and Walter, 1997). We thus asked if a loss of either Ire1 or Hac1 would affect the increase in the number of ERMES dots under ER-stress conditions. The loss of Ire1 or Hac1 did not suppress the increase in the number of ERMES dots (Figures 3A and 3C). These findings suggest that the ER-stress dependent change in the ERMES dot number represents a non-canonical response to deal with the ER stress. We confirmed that tunicamycin treatment did not affect the protein levels of ERMES components such as Mmm1 and Mdm12, although it decreased the level of N-glycosylated forms of Mmm1 and Mmm1-GFP (Figure S2). Therefore, the sharp increase in the number of ERMES dots was not because of the increased expression of the ERMES components. Rather, more likely explanation for the increased number of ERMES dots is that the ERMES dots dissociate on ER stress. Indeed, we confirmed that the estimated numbers of Mmm1-GFP molecules present in an ERMES dot after the tunicamycin or DTT treatment were lower than that in nontreated wild-type cells (Figure 3D). The use of super-resolution confocal live imaging microscopy (SCLIM) enabled us to obtain time-lapse fluorescent images of whole yeast cells at super-high resolution (Kurokawa et al., 2013,2014), which showed the splitting of the ERMES dot taking place after tunicamycin treatment (Figure 3E, Videos S1, S2, S3, and S4). These findings strongly suggest that dissociation of ERMES dots is responsible for the observed increase in the ERMES dot number. Because the increased ERMES dot number returned to the normal level in 4 h after washing out of DTT (Figure 3F), the dissociation and association of ERMES dots depending on the ER stress are reversible processes. These results also suggest that ERMES dots are stable entities that can congregate or divide. Supporting this idea, a previous study revealed that the ERMES dot is a stable structure by FRAP analysis (Nguyen et al., 2012).

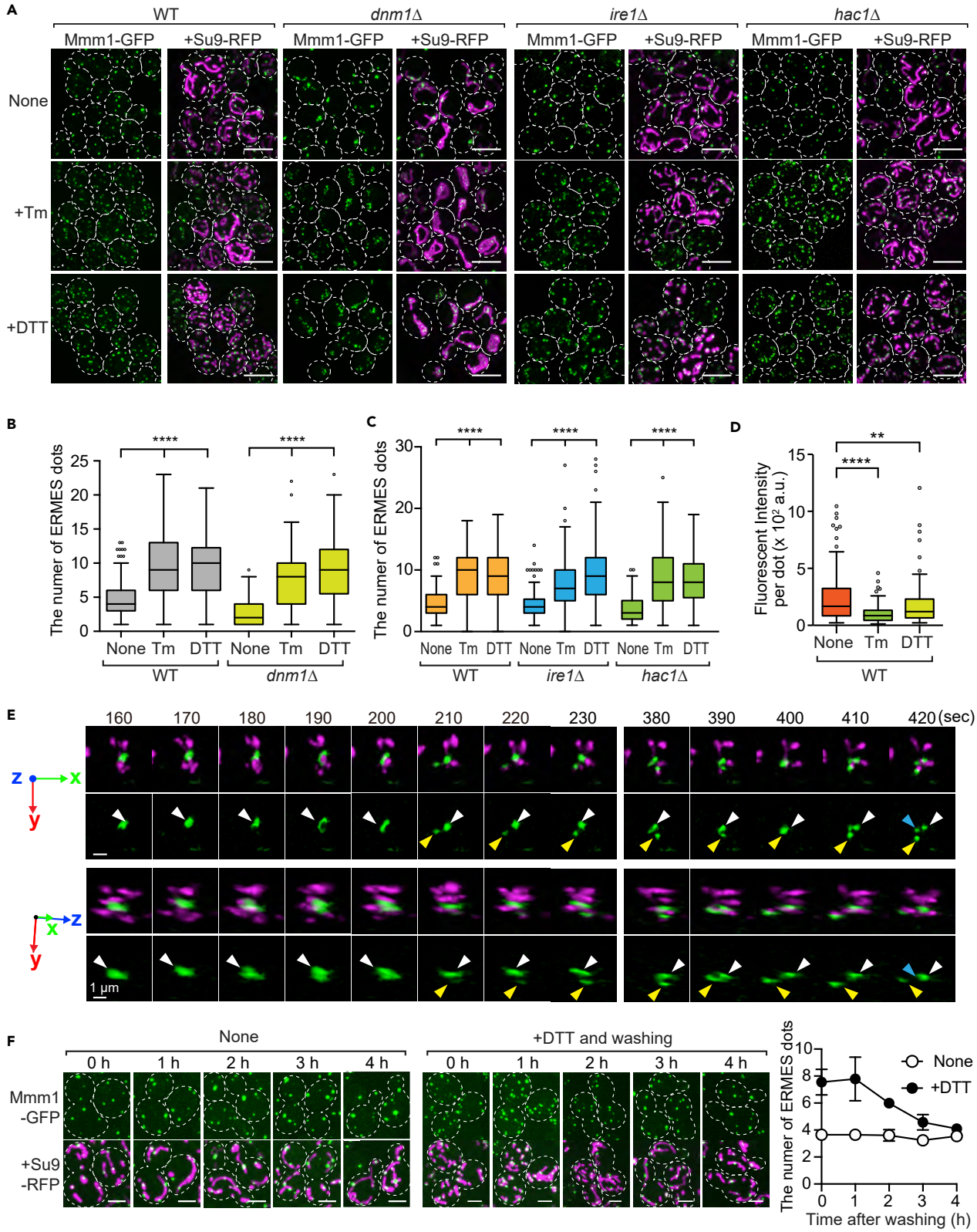
A
WT
dnm1Δ
ire1Δ
hac1Δ
Mmm1-GFP
+Su9-RFP
None
+Tm
+DTT
B
The numer of ERMES dots
None Tm DTT None Tm DTT
WT
dnm1Δ
C
The numer of ERMES dots
WT
ire1Δ
hac1Δ
D
Fluorescent Intensity per dot (x 10² a.u.)
E
160 170 180 190 200 210 220 230 380 390 400 410 420 (sec)
1 μm
F
None
+DTT and washing
0 h 1 h 2 h 3 h 4 h
Mmm1 -GFP
+Su9 -RFP
The numer of ERMES dots
Time after washing (h)

Figure 3. The number of ERMES dots significantly increases on treatments with ER stress inducers independently of mitochondrial division and the conventional UPR pathway

(A) Wild-type (WT), *dnm1Δ*, *ire1Δ*, and *hac1Δ* cells expressing Mmm1-GFP and mitochondria-targeted RFP (Su9-RFP) were incubated with or without 1 μg/mL tunicamycin (+Tm) or 3 mM DTT (+DTT) for 2 h, and were observed using confocal fluorescence microscopy. Maximum projection images reconstituted from z-stacks were shown. Scale bars denote 5 μm.

(B) Box and whisker plots show the number of ERMES dots per wild-type and *dnm1Δ* cell with or without the treatment inducing ER stress. n = 199, 194, and 132 (WT, None, Tm, and DTT), n = 179, 174, and 105 (*dnm1*Δ, None, Tm, and DTT), ****p< 0.0001.

(C) Box and whisker plots show the number of ERMES dots per wild-type and *ire1Δ*, or *hac1Δ* cell with or without the treatment inducing ER stress. n = 150, 150, and 131 (wild-type, None, +Tm and +DTT), n = 150, 150, and 150 (*ire1*Δ, None, +Tm and +DTT), and n = 150, 150, and 142 (*hac1*Δ, None, +Tm and +DTT). ****p< 0.0001.

(D) Quantifications of signal intensities of ERMES dots in wild-type cells with or without the DTT or Tm treatment as in Figure 1C. **p = 0.0019 and ****p< 0.0001; p values were obtained from the unpaired two-tailed t-test with Welch's correction (B–D).

(E) Three-dimensional time-lapse images of yeast cells that chromosomally express Mmm1-GFP and Idh1-RFP were taken at 10-s intervals by SCLIM (see also Videos S1, S2, S3, and S4). Upper and lower panels indicate the same ERMES dot at different angles. Arrow heads with different colors indicate distinct ERMES dots. Scale bar denotes 1 μm.

(F) Wild-type cells expressing Mmm1-GFP and mitochondria-targeted RFP (Su9-RFP) were incubated in SCD medium with or without 3 mM DTT for 2 h. The cells were washed with SCD medium, and observed using confocal fluorescence microscopy after cultivation for the indicated times. Maximum projection images reconstituted from z-stacks were shown. Scale bars denote 5 μm. The number of ERMES dots in approximately 100 cells was counted. Values are means ± SD (n = 3).

Dissociation of the ERMES complex causes a decrease in lipid transport activity

The next question we asked was what the physiological relevance of the dissociation of ERMES complexes was. Given the lipid-transfer function of ERMES and the ER membrane expansion under the ER stress condition, the ER stress-dependent change in the ERMES clustering could affect the phospholipid metabolism. To test this, we metabolically labeled yeast total phospholipids with ^{32}Pi, with or without induction of the ER stress, and analyzed the radio-active phospholipids by thin-layer chromatography followed by radio imaging. Interestingly, we found that the accumulation of phosphatidylserine (PS) was impaired under the ER stress conditions whereas other phospholipids were comparably produced irrespective of the ER stress (Figures 4A, 4B, and S3A). This suggests that the impaired PS accumulation triggered the ERMES dissociation, or ER stress-dependent factors including altered ERMES clustering affected the PS metabolism. To obtain insights into these possibilities, we tested if impaired PS synthesis directly affected the appearance of ERMES dots. When Cho1 PS synthase was depleted, we did not see a significant change in the number of ERMES dots (Figure S3B), suggesting that the ERMES dissociation affected the phospholipid metabolism. To further confirm this interpretation, we asked if the phospholipid transport between the ER and mitochondria was altered under ER stress conditions. To this end, we performed pulse-chase experiments using *psd2Δdpl1*Δ cells. In *psd2Δdpl1Δ* cells, Psd1, which is located in the MIM, is the sole enzyme involved in the production of phosphatidylethanolamine (PE) through the decarboxylation of PS synthesized in the ER (Clancey et al., 1993). Therefore, PS transport from the ER to mitochondria can be assessed by monitoring the conversion of PS to PE as an index. In addition, because the conversion of PE to PC occurs only in the ER, we can assess PE transport from mitochondria to the ER by monitoring the PE to PC conversion as an index (Figure 4C). We pulse-labeled PS with ^{14}C-serine in *psd2Δdpl1*Δ cells, and compared its conversion to PE and PC under normal and ER stress conditions. Consistent with the results of metabolic labeling of phospholipids with ^{32}Pi, the tunicamycin or DTT treatment diminished the PS synthesis (Figures 4D and 4E, Total). Besides, we found that the PS transport from the ER to mitochondria, as assessed by the PS ratio relative to total phospholipid, was slowed under the ER stress conditions (Figures 4D and 4E, PS/total). The conversion of PE to PC was also decreased under the ER stress condition (Figures 4D and 4E, PC/total), indicating that PE export from mitochondria to the ER was compromised, as well. We obtained similar results when we performed *in vitro* phospholipid transport assay (Kojima et al., 2016). Briefly, we synthesized radio-active PS by incubating ^{14}C-serine with heavy membrane fractions containing both ER and mitochondria membranes isolated from yeast cells with or without the ER stress, and observed its conversion to PE and PC. The results also support the idea that PS transport from the ER to mitochondria was decelerated in membranes isolated under ER stress conditions (Figures 4F and 4G, PS/total). Alternatively, the conversion of PE to PC may not necessarily reflect the PS transport from the ER to mitochondria, because Psd1 is also localized to the ER. (Friedman et al., 2018). However, most Psd1 was detected as a mitochondria-localized form, whereas only a small amount of ER-localized Psd1 was found in the heavy membranes (Figure 4L) (Sam et al., 2021). We also confirmed that amounts of phospholipid synthetic enzymes such as Cho1, Psd1, Cho2, and Opi3 were comparable or increased in the membrane fractions isolated from DTT- or tunicamycin-treated cells compared with those of control membranes (Figure 4L). These results strongly suggest that the dissociated ERMES complexes have less activity to

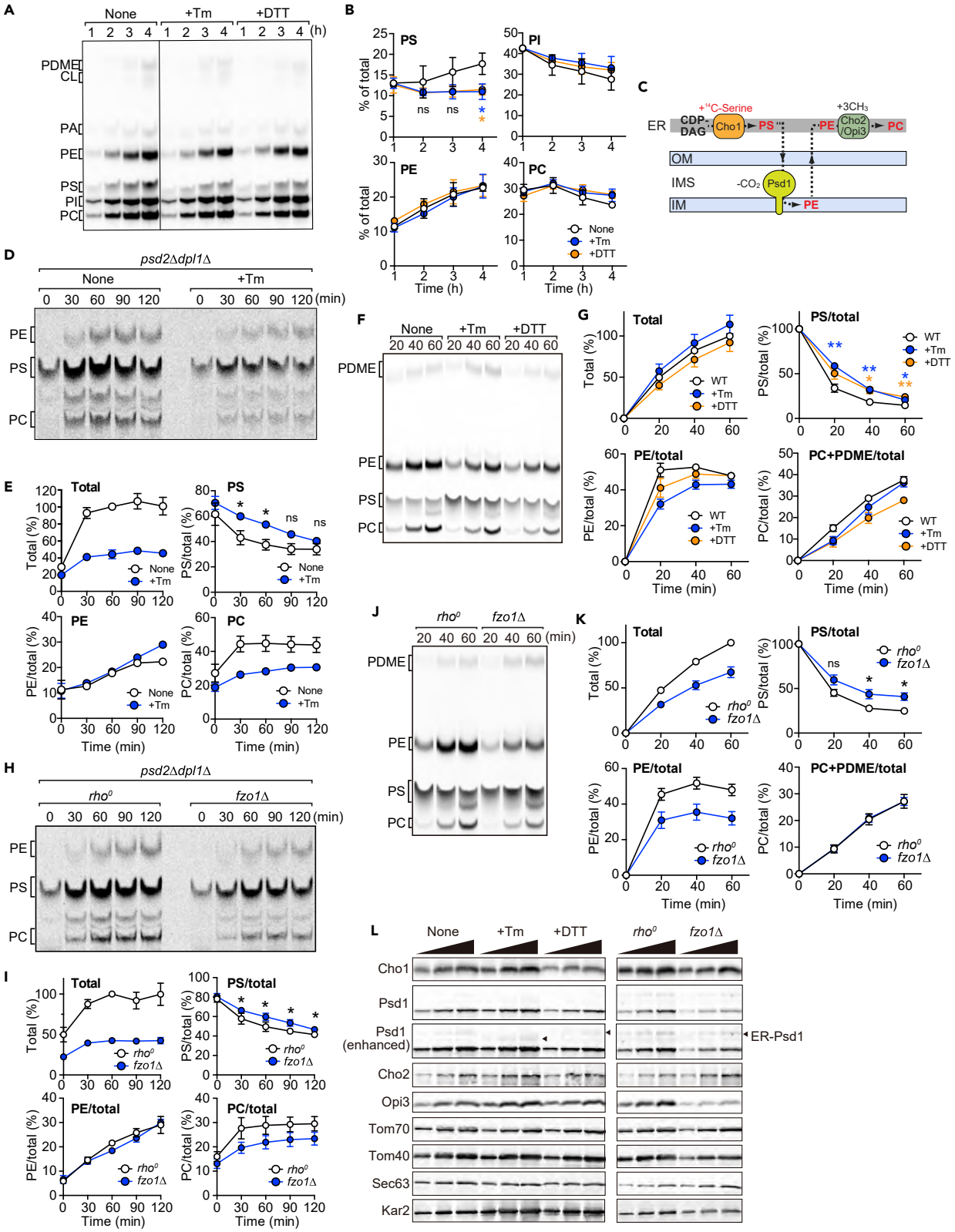
A
None
+Tm
+DTT
1 2 3 4 1 2 3 4 1 2 3 4 (h)
PDME
CL
PA
PE
PS
PI
PC
B
PS
PI
PE
PC
% of total
Time (h)
ns
None
+Tm
+DTT
C
ER
CDP-DAG
Cho1
PS
PE
Cho2 /Opi3
PC
+14C-Serine
+3CH3
OM
IMS
-CO2
Psd1
IM
D
psd2Δdpl1Δ
None
+Tm
0 30 60 90 120 0 30 60 90 120 (min)
PE
PS
PC
E
Total
PS
PE
PC
Total (%)
PS/total (%)
PE/total (%)
PC/total (%)
Time (min)
F
None
+Tm
+DTT
20 40 60 20 40 60 20 40 60
PDME
PE
PS
PC
G
Total
PS/total
PE/total
PC+PDME/total
WT
+Tm
+DTT
Time (min)
H
psd2Δdpl1Δ
rho0
fzo1Δ
0 30 60 90 120 0 30 60 90 120 (min)
I
Total
PS/total
PE/total
PC/total
rho0
fzo1Δ
Time (min)
J
rho0
fzo1Δ
20 40 60 20 40 60 (min)
PDME
PE
PS
PC
K
Total
PS/total
PE/total
PC+PDME/total
rho0
fzo1Δ
Time (min)
L
None
+Tm
+DTT
rho0
fzo1Δ
Cho1
Psd1
Psd1 (enhanced)
ER-Psd1
Cho2
Opi3
Tom70
Tom40
Sec63
Kar2

Figure 4. ER stress alters phospholipid metabolism

(A) Total phospholipids of logarithmically growing wild-type cells were labeled with ^{32}Pi for the indicated time in the presence or absence of 1 μg/mL tunicamycin (+Tm) or 3 mM DTT (+DTT) and were analyzed by TLC and autoradiography.

(B) The ratio of PS, PE, PI, or PC relative to the total labeled phospholipids was determined at each time-point and plotted. Values are means ± S.E. (n = 3). *: p< 0.05, p values were obtained from the unpaired two-tailed t-test. ns: not significant.

(C) A schematic diagram for the phospholipid transport and synthesis between the ER and mitochondria.

(D) Logarithmically growing *psd2Δdpl1Δ* cells in YPD medium were treated with 1 μg/mL tunicamycin (+Tm) or dimethyl sulfoxide (None) for 2 h. The cells were incubated in PBS containing ^{14}C-serine for 15 min, washed once with YPD, and further incubated in YPD medium with or without 1 μg/mL tunicamycin for the indicated times. Total phospholipids were extracted and analyzed by thin-layer chromatography followed by radioimaging.

(E) The ratio of PS, PE, or PC relative to the total labeled phospholipids was determined at each time-point and plotted. Values are means ± S.E. (n = 3). *: p< 0.05, p values were obtained from the unpaired two-tailed t-test. ns: not significant.

(F) Heavy membrane fractions were isolated from wild-type yeast cells and incubated with ^{14}C-serine for the indicated times. Total phospholipids were extracted and analyzed by TLC and radioimaging.

(G) Amounts of PS, PE and PDME+ PC relative to total phospholipids were calculated and plotted. Values are mean ± SEM (n = 4). The amount of total phospholipids synthesized with the wild-type membranes after 60-min incubation was set to 100% (Total) *: p< 0.05, **: p< 0.01, p values were obtained from the unpaired two-tailed t-test.

(H) *In vivo* pulse-chase experiments were performed as in (D) using *psd2Δdpl1Δrho^0* and *psd2Δdpl1Δfzo1Δ* cells.

(I) The amounts of PS, PE, or PC detected in (H) were quantified and their ratios relative to the total labeled phospholipids at each time-point were plotted. Values are means ± S.E. (n = 3). *: p< 0.05, p values were obtained from the unpaired two-tailed t-test.

(J) *In vitro* phospholipid transfer assays were performed as in (F) using heavy membrane fractions isolated from *rho^0* and *fzo1Δ* cells.

(K) Quantifications of phospholipids detected in (J) were performed as in (G). Values are mean ± SEM (n = 4). *: p< 0.05, p values were obtained from the unpaired two-tailed t-test. ns: not significant.

(L) The heavy membrane fractions used in (F) and (J) were subjected to immunoblotting using antibodies against the indicated proteins. For clear visualization of the ER-localized Psd1, enhanced images of Psd1 were shown. Arrowheads indicate the ER-localized Psd1.

transport phospholipid. However, it is still possible that the impaired phospholipid transport is a secondary effect of the ER stress and is not directly associated with the ERMES dissociation.

To answer the above question, we performed the same *in vivo* and *in vitro* assays to assess phospholipid transport between the ER and mitochondria using *fzo1Δ* cells in which the ERMES complexes become smaller independently of the ER stress (Figure 1A). We pulse-labeled *psd2Δdpl1Δrho^0* and *psd2Δdpl1Δfzo1Δ* cells with ^{14}C-serine and chased the fate of synthesized PS. Similar to the case when cells were treated with tunicamycin, the loss of Fzo1 decelerated PS transport from the ER to mitochondria (Figures 4H and 4I). We also obtained similar results when we analyzed the phospholipid transport *in vitro* (Figures 4J and 4K). Immunoblotting of the membrane fractions indicated that the steady state levels of Psd1 and Opi3 were reduced in the absence of Fzo1, suggesting that the observed delay of the PS to PE conversion is because of the decreased Psd1 level but not because of the defects in the PS transport from the ER to mitochondria (Figure 4L). Notably, we confirmed that the PS transport was still impaired when Psd1 was overexpressed (Figures S3C and S3D). This result shows that the PS transport is the rate-limiting step in PE synthesis and the effect of the ER-localized Psd1 on the PE synthesis is negligible in the *in vitro* assay. Taken these results together, we propose that the proper ERMES clustering is critical for the efficient phospholipid transport between the ER and mitochondria.

ER stress leads to ER membrane expansion through ERMES functions

Our findings suggest that the functions of ERMES in lipid trafficking may be two-fold. One is a direct role in phospholipid transfer by passive diffusion between the ER and MOM, which should be critical for normal cell growth. In addition to this function, the present findings suggest that ERMES may contribute to the response to the ER stress, which is mediated by dissociation of the large ERMES dots and is associated with modulation of phospholipid transport. To discriminate these two functions of ERMES, we looked for a way to suppress the dissociation of ERMES dots, without affecting the direct lipid-transfer function of the ERMES complex. Interestingly, we happened to find that the ER stress-dependent increase in the ERMES dot number visualized with Mdm12-GFP was significantly suppressed in *mmm1-1*, a temperature-sensitive mutant of Mmm1, at a permissive temperature 23°C (Figures 5A and 5B), where the ERMES-mediated lipid transport directly related to the cell growth is not compromised (Figure S4). We found that *mmm1-1* cells became more susceptible to the tunicamycin treatment with respect to the cell growth as compared with the corresponding wild-type cells on agar plates and in liquid media (Figure 5C). Thus, the *mmm1-1*mutant could offer a useful tool to analyze the two distinct roles of EMRES, direct lipid transfer and ER stress response, separately.

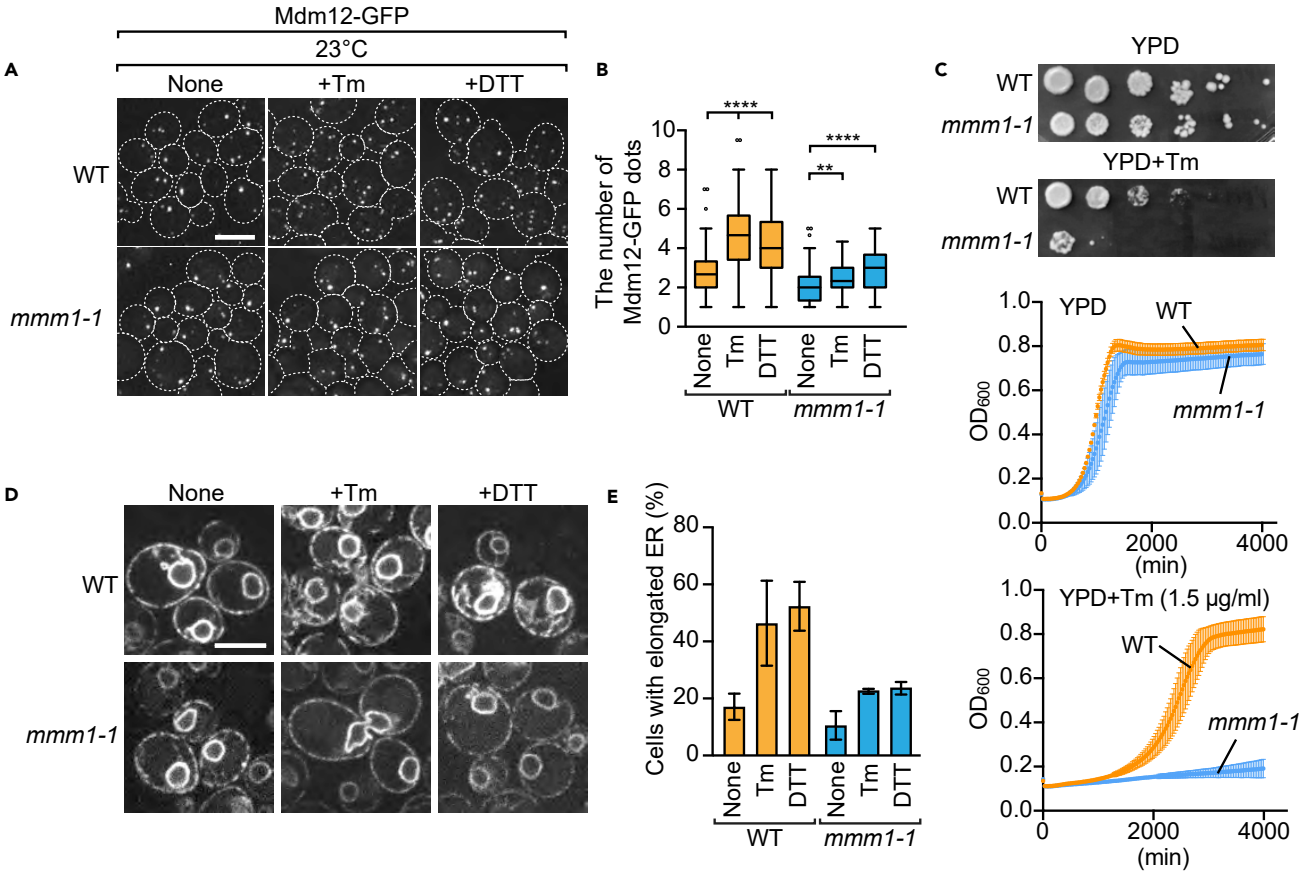

Figure 5. ER stress causes membrane expansion in an Mmm1-dependent manner

(A) *mmm1-1* and the corresponding wild-type cells expressing Mdm12-GFP were incubated in SCD medium at 23°C with or without 1 μg/mL tunicamycin (+Tm) or 3 mM DTT (+DTT) for 2 h, and then observed using confocal fluorescence microscopy. Maximum projection images reconstituted from z-stacks are shown. Scale bars denote 5 μm.

(B) Box and whisker plots show the number of ERMES dots visualized by Mdm12-GFP per wild-type cell with or without the treatment inducing ER stress. Numbers above the plots show the mean values. n = 269, 209, and 219 (WT, None, Tm, and DTT, respectively) and n = 218, 233, and 176 (*mmm1-1*, None, Tm, and DTT, respectively). ****p< 0.0001 and **p = 0.0057; p values were obtained from the unpaired two-tailed t-test with Welch's correction.

(C) Serial dilutions of *mmm1-1* and its corresponding wild-type cells were spotted onto YPD medium with or without 1 μg/mL tunicamycin (+Tm) at 23°C. The growth curves were recorded while these cells were cultured in a plate reader.

(D) Wild-type and *mmm1-1* cells expressing the ER-targeted GFP were incubated in SCD medium at 23°C with or without 1 μg/mL tunicamycin (+Tm) or 3 mM DTT (+DTT) for 2 h and then observed using confocal fluorescence microscopy. A single optical slice around the center of cells is shown for each condition. Scale bars denote 5 μm.

(E) Ratio of cells containing the expanded ER membranes. A total of over 180 cells were evaluated by three independent experiments. Values are mean ± S.E. (n = 3).

What is the mechanism of the ER stress response mediated by dissociation of large ERMES dots? Since previous studies showed that the ER membranes were significantly expanded on ER stress (Schuck et al., 2009; Sriburi et al., 2004), we examined whether the *mmm1-1*mutation affected the ER expansion. Interestingly, the ER stress-dependent ER membrane expansion was partly suppressed in *mmm1-1* cells at a permissive temperature of 23°C (Figure 5D). After 2 h-ER stress inductions, ~ 50% of wild-type cells showed the ER structure with elongated shapes, whereas only ~20% of *mmm1-1* cells contained such a developed ER structure (Figure 5E). Although the *mmm1-1* mutation, which causes defective dissociation of the ERMES large dots, does not affect the basal level of the phospholipid flux between the ER and mitochondria at permissive temperature (Figure S4), it could affect further decrease in the phospholipid flux that is required for transient expansion of the ER membrane as a response to the ER stress. It is known that Ino2/Ino4 transcription factors, which activate transcription of a series of genes for phospholipid synthases, are upregulated in a Hac1-dependent manner under the ER stress conditions, and play a critical role in the ER membrane expansion (Cox et al., 1997; Henry et al., 2012; Schuck et al., 2009). In particular, the loss of Ino2, Ino4,

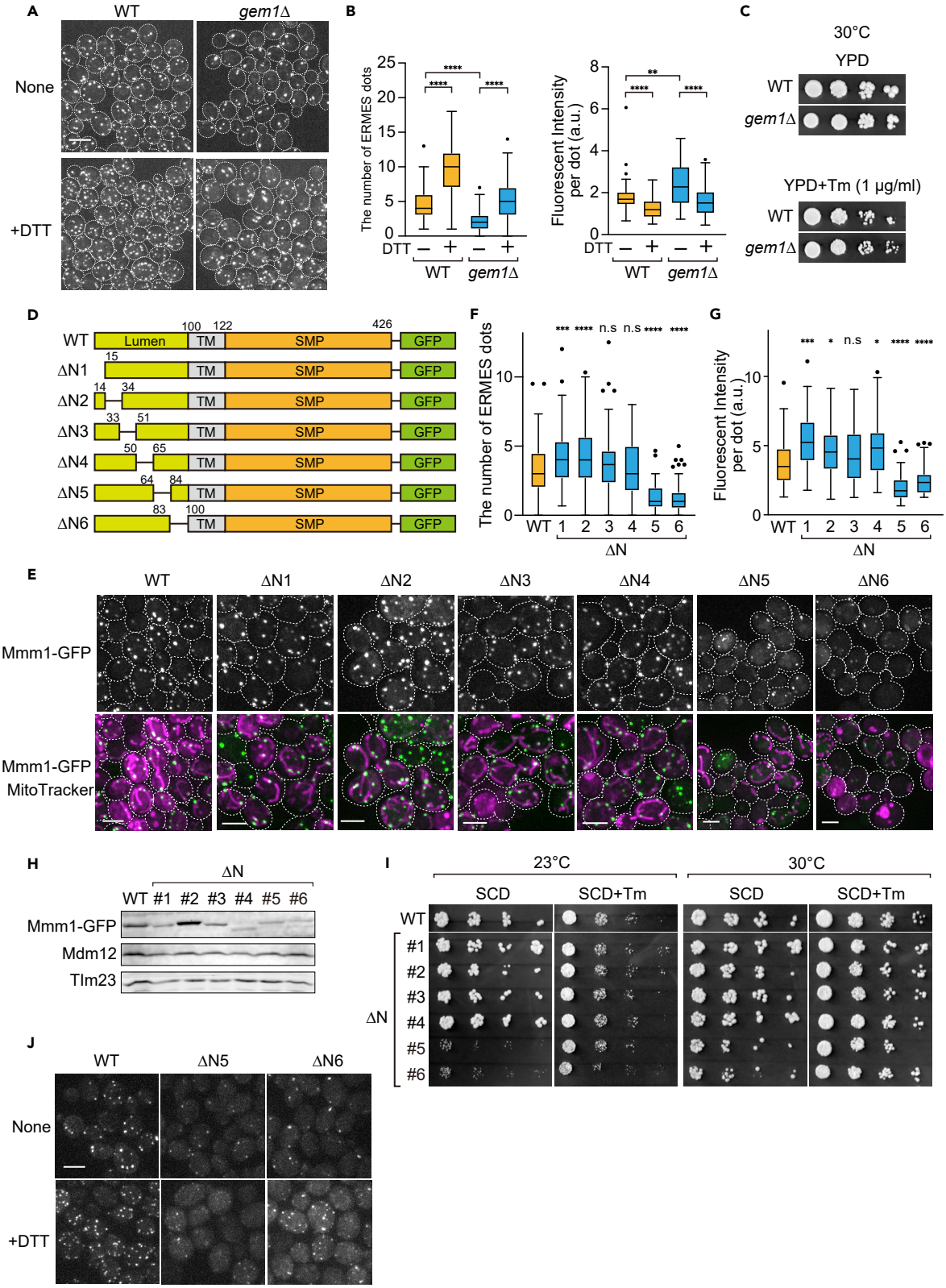
A
WT
gem1Δ
None
+DTT
B
The number of ERMES dots
Fluorescent Intensity per dot (a.u.)
DTT
WT
gem1Δ
C
30°C
YPD
YPD+Tm (1 μg/ml)
D
Lumen
TM
SMP
GFP
ΔN1
ΔN2
ΔN3
ΔN4
ΔN5
ΔN6
E
Mmm1-GFP
Mmm1-GFP
MitoTracker
F
G
ΔN
H
Mmm1-GFP
Mdm12
Tim23
I
23°C
30°C
SCD
SCD+Tm
J

Figure 6. Gem1 and the ER-lumenal domain of Mmm1 are involved in the ERMES clusering

(A) Wild-type and *gem1Δ* cells expressing Mmm1-GFP were imaged under a confocal fluorescence microscope. Maximum projection images were shown. Scale bars, 5 μm.

(B) Box and whisker plots show the distribution of the number of ERMES dots per cell (left) and relative fluorescent signals per a single ERMES dot. n = 225, 219, 281 and 233 (WT ± DTT, *gem1Δ* WT ± DTT)(left), n = 156, 155, 153 and 157 (WT ± DTT, *gem1Δ* WT ± DTT)(right). **p = 0.0010, ****p< 0.0001, p values were obtained from the unpaired two-tailed t-test with Welch's correction.

(C) Wild-type and *gem1Δ* cells were spotted onto YPD medium with or without 1 μg/mL tunicamycin (+Tm) and cultivated at 30°C for 2 (YPD) and 6 days (YPD + Tm).

(D) Schematics of Mmm1 mutants lacking a part of the ER-lumenal domain.

(E) The indicated yeast cells expressing Mmm1-GFP mutants were imaged under a confocal fluorescence microscope. Mitochondria were stained with MitoTracker. Maximum projection images were shown. Scale bars, 5 μm.

(F and G) Box and whisker plots show the distribution of the number of ERMES dots per cell, and the relative fluorescent signals per a single ERMES dot, respectively. n = 387, 271,337, 286, 195, 206, and 269 (WT, ΔN1-6) ***p = 0.005, ****p< 0.0001 (left), n = 152, 151, 152, 152, 151, 150, and 151 (WT, ΔN1-6) (right). *p = 0.016, ***p = 0.0001, ****p< 0.0001.

(H) Immunoblotting of total cell lysates isolated from the indicated cells were shown.

(I) Wild-type and the indicated mutant cells were spotted onto YPD medium with or without 1 μg/mL tunicamycin (+Tm) and cultivated at 23 and 30°C.

(J) Mmm1-GFP, Mmm1-ΔN5 or-ΔN6-GFP expressing cells were imaged under a confocal fluorescence microscope. Maximum projection images were shown. Scale bars, 5 μm.

or Hac1 diminished the ER membrane expansion under the ER stress conditions (Schuck et al., 2009). Then, the *ino2*Δ, *ino4*Δ, or *hac1*Δ mutation may first abolish the increase in the ERMES dot number, which would subsequently diminish the ER membrane expansion. However, we observed that the tunicamycin or DTT treatment resulted in a similar increase in the number of ERMES dots in *ino2*Δ, *ino4*Δ, or *hac1*Δ cells (Figure S5). This suggests that upregulation of Ino2 and Ino4 and dissociation of large ERMES complexes operate in parallel to expand the ER membranes on ER stress (Figure 6). In other words, the ERMES dissociation may play a role in retaining phospholipids, which are actively synthesized under the ER stress condition, in the ER, thereby contributing to the ER membrane expansion for attenuating the stress.

Possible mechanisms of the ERMES cluster dissociation

What mechanism underlies the dissociation of ERMES dots under ER stress conditions? Previous studies found Gem1 and Emr1 as regulators of the ERMES clustering (Kornmann et al., 2011; Rasul et al., 2021) Loss of either factor was reported to decrease the number of ERMES dots and increase their size. We thus tested whether Gem1 and Mco6, a budding yeast ortholog of Emr1, would affect the ERMES dissociation under the ER stress conditions. As reported previously, the loss of Gem1 reduced the number of ERMES dots and increased their size, but it did not suppress the significant increase in the ERMES dot number under the ER stress condition (Figures 6A and 6B). The growths of *gem1*Δ cells were comparable to the wild-type cells in the presence or absence of tunicamycin (Figure 6C). These results indicate that Gem1 is indeed involved in regulation of ERMES clustering while it is dispensable for the dissociation of ERMES dots under the ER stress condition. Besides, we confirmed that the number and size of ERMES dots in the absence of Mco6 were similar to those of wild-type cells, suggesting that the role of Mco6 in controlling the ERMES clustering is minor in budding yeast (Figure S6A).

Another possibility is that the ER stress leads to dissociation of ERMES dots through modifications, such as phosphorylation and ubiquitination of the ERMES components. However, we did not observe obvious band shifts for at least Mmm1 and Mdm12 among ERMES components by SDS-PAGE followed by immunoblotting (Figure S2). We also confirmed that yeast cells expressing Mdm34-3PA mutant, which lacks the PY motif critical for its ubiquitination by Rsp5 E3 ubiquitin ligase, showed a similar increase in the ERMES dot number after tunicamycin and DTT treatments (Figure S6B) (Belgareh-Touzé et al., 2017).

Moreover, we reasoned that the accumulation of abnormal proteins in the ER lumen because of ER stress might be a factor causing the dissociation of ERMES dots and the ER-lumenal domain of Mmm1 could sense the abnormal environment. We thus generated several deletion mutants of a part of the ER-lumenal domain (15–20 amino acid residues) of Mmm1 and examined whether the partial deletion affected the ERMES clustering (Figure 6D). Among the deletion mutants we tested, Mmm1-ΔN5 and ΔN6, which lacked amino acid residues 65–83 and 84–99, respectively, showed impaired formation of ERMES dots (Figures 6E and S6C). Both the number and size of the ERMES dots were smaller in the mutant cells expressing Mmm1-ΔN5 or ΔN6 than those of wild-type control cells (Figures 6F and 6G). Immunoblotting of total lysates prepared from the Mmm1-deletion mutants showed that the levels of Mmm1-ΔN5 and ΔN6 were smaller than that of wild-type but comparable with those of Mmm1-ΔN1, ΔN3 and ΔN4 mutants. The levels of Mdm12

were similar among the Mmm1-deletion mutants. These results indicate that the defective formation of ERMES dots was not simply because of the destabilization of Mmm1-GFP and Mdm12 (Figure 6H). Although the Mmm1-ΔN5 and ΔN6 mutant cells showed cold-sensitive growth defects, they did not become more susceptible to tunicamycin. Besides, the Mmm1-ΔN5 and ΔN6 mutants retained the ability to dissociate on ER stress. These results indicate that the lumenal domain of Mmm1 is important for ERMES clustering but not essential for the ER stress-dependent dissociation of ERMES dots.

DISCUSSION

In the present study, we attempted to analyze the likely important, but previously overlooked aspects of regulation of the ERMES dot number in a yeast cell. We found that the number and size of the ERMES dots are determined by the association and dissociation of ERMES dots. A small number of large ERMES dots and the large number of small dots were observed in yeast mutants deficient in the mitochondrial division and fusion, respectively. This means that the clustering and unclustering of the ERMES subclusters and clusters, respectively, are associated with the mitochondrial fusion and division, which antagonistically regulate the number of the ERMES dots. It is not clear, however, if division and fusion-associated changes in the ERMES dot numbers are regulated actively by specific factors.

We also found that large ERMES dots become dissociated into smaller sub-clusters in response to the ER stress, which is independent of the canonical Ire1/Hac1 pathway. This ER-stress dependent dissociation of ERMES dots looks reversible because the ERMES dot numbers are restored after removal of the cause for the ER stress (Figure 3F). Of interest, microscopic observation suggests that the preexisting ERMES dots contacted with each other to form large aggregates (Figure 2D). In addition, our live cell imaging analyses captured repeated dissociation and association of the ERMES dots, suggesting that these contacts of ERMES dots appeared reversible, as well (Videos S1, S2, S3, and S4). These findings indicate the principle of the dynamic nature of ERMES, that is, ERMES dots can reversibly dissociate into smaller sub-clusters or in turn, sub-clusters assemble into large ERMES dots.

The ERMES protein complex is thought to play an essential role in phospholipid trafficking between mitochondria and the ER, which is critical for yeast cell growth. This inter-organelle lipid transfer function of ERMES is mediated by the cooperative action of the SMP domains of Mmm1 and Mdm12 (Kawano et al., 2018), and likely that of Mdm34, as well. In addition to this, the present results point to a possible role of EMRES in the ER stress response through the dynamic change in the ERMES clustering, which further affects the phospholipid trafficking (Figure 7). Supporting this idea, our results clearly indicated that the PS transfer from the ER to mitochondria was impaired when the size of ERMES dots was small. Therefore, the dissociation of large ERMES dots may limit the amounts of phospholipids passing through ERMES above the basal flux level. This would then result in phospholipid accumulation in the ER, which may lead to the ER membrane expansion. Such regulation of the phospholipid flux may be achieved by controlling the amounts of phospholipids transiently accumulated or pooled in the SMP domains in the aggregated ERMES dots (Tamura et al., 2020). In summary, we propose that, together with the transcriptional activation through the Ire1/Hac1 pathway, lipid accumulation in the ER because of lowered phospholipid efflux from the ER via ERMES dots may cooperatively contribute to the ER membrane expansion to buffer the ER stress (Figure 7).

Although our findings shed light on the ERMES-mediated pathway of ER stress response, several unresolved issues remain. For example, it is unclear how Ino2/Ino4 transcription factors are activated in Ire1/Hac1-dependent manner on ER stress. A previous study suggests a possibility that Hac1 inhibits the function of Opi1 as a repressor for Ino2/Ino4 although this has not yet been revealed (Cox et al., 1997). Besides, we could not obtain clear insight into what triggers the dissociation of ERMES dots. Although we found that *mmm1-1* mutant fails to dissociate ERMES clusters and expand the ER membrane in response to ER stress at the permissive temperature (Figure 5), it is completely unknown why this mutation affects the ERMES clustering at this point. *mmm1-1* mutant carries the S252D mutation. According to the Alpha-fold structure of Mmm1, S252 is located on the protein surface (Jumper et al., 2021). Therefore, the D252S mutation may contribute to stabilize the interaction between the ERMES sub-clusters at the permissive temperature although the ERMES dots are gone at over 30°C. As reported previously, Gem1 was indeed involved in proper clustering of ERMES, but was not critical for the ER stress response via dissociation of ERMES dots (Figures 6A–6C). Although we found that the lumenal domain of Mmm1 is critical for the ERMES clustering, its deletion mutant could still respond the ER stress (Figures 6I and 6J). Furthermore, although we

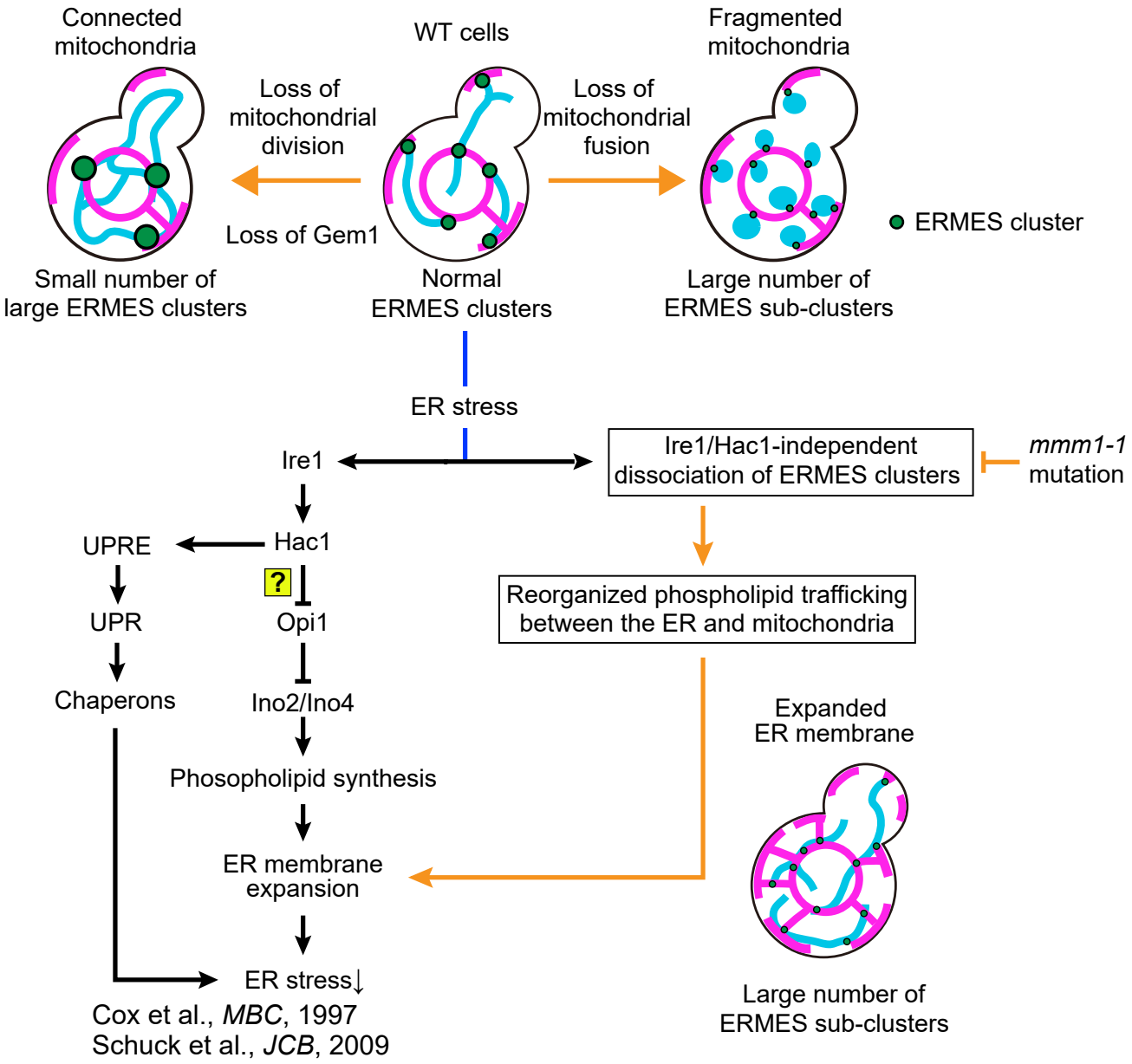

Figure 7. A model for the ER stress response

Orange arrows and the area enclosed in a square indicate the processes found in this study. Question mark indicates that the Ire1/Hac1-dependent activation of Ino2/Ino4, which was suggested but not examined experimentally (Cox et al., 1997).

confirmed that defective PS synthesis did not cause the dissociation of ERMES dots (Figure S3), it is still possible that acyl-chain variations cause changes in packing of the ERMES complexes in its clusters, which may lead to their dissociation. Alternatively, protein modifications or additional binding partners for ERMES subunits may cause the dissociation of ERMES dots under ER stress conditions. Future studies should reveal the detailed mechanisms underlying the dynamic feature of the number of ERMES dots to answer these questions.

Limitations of the study

Although we showed that the PS transport from the ER to the mitochondria was impaired under ER stress conditions, the degree of inhibition was not quite large. Therefore, it is unclear whether the impaired PS transport alone can explain the expansion of the ER membrane under ER stress conditions. The *in vivo*

and *in vitro* lipid transport experiments can only evaluate the PS transport from the ER to mitochondria but not the transport of other phospholipids. Because this is a limitation of this study, it will be important to investigate whether the transport of phospholipids other than PS is indeed suppressed during ER stress. In addition, the ERMES complex is not fully conserved in higher eukaryotes. Therefore, it will also be important to ascertain whether some aspects of the ER-mitochondrial contact sites obtained in this study using yeast are also conserved in other higher eukaryotic systems.

STAR★METHODS

Detailed methods are provided in the online version of this paper and include the following:

- KEY RESOURCES TABLE
- RESOURCE AVAILABILITY
  - Lead contact
  - Materials availability
  - Data and code availability
- EXPERIMENTAL MODEL AND SUBJECT DETAILS
- METHOD DETAILS
  - Strains, plasmids, primers, and growth conditions
  - Fluorescence microscopy
  - Immunoblotting and antibodies
  - *In vivo* pulse-chase experiment with ^{14}C serine
  - *In vitro* phospholipid transport assay with ^{14}C serine
- QUANTIFICATION AND STATISTICAL ANALYSIS

SUPPLEMENTAL INFORMATION

Supplemental information can be found online at https://doi.org/10.1016/j.isci.2022.105362.

ACKNOWLEDGMENTS

We thank M. Hashimoto, and T. Sasaki for their great technical assistance and Profs. Robert E. Jensen and Hiromi Sesaki for *mmm1-1* and its corresponding wild-type strain. We are grateful to the members of the Tamura and Endo laboratories for helpful discussion. This work was supported by JSPS KAKENHI (Grant Numbers 17H06414 and 19H03174 to YT, 17H06413, 17H06420 and 18H05275 to K.K and AN, and 15H05705 and 22227003 to TE), AMED-PRIME (Grant Number JP20gm5910026) from Japan Agency for Medical Research and Development, AMED and the Naito Foundation to YT, and a CREST Grant (JPMJCR12M1) from JST, an AMED-CREST grant (21gm1410002h0002) from AMED, and a grant from Takeda Science Foundation to TE. YKT was a JSPS fellow.

AUTHOR CONTRIBUTIONS

Conceptualization, Y.T.; Methodology, K.K., A.N., and Y.T.; Investigation, Y.K-T., R.K., Y.T., H.S., and K.K; Writing – Original Draft, Y.T.; Writing – Review & Editing, Y.K-T., R.K., T.E, K.K., A.N., and Y.T.; Funding Acquisition, T.E, K.K., A.N., and Y.T.; Resources, T.E.; K.K., A.N., and Y.T.; Supervision, T.E. and Y.T.

DECLARATION OF INTERESTS

The authors declare no competing interests.

Received: May 16, 2022
Revised: August 24, 2022
Accepted: October 12, 2022
Published: November 18, 2022

REFERENCES

Di Bartolomeo, F., Malina, C., Campbell, K., Mormino, M., Fuchs, J., Vorontsov, E., Gustafsson, C.M., and Nielsen, J. (2020). Absolute yeast mitochondrial proteome quantification reveals trade-off between biosynthesis and energy generation during diauxic shift. Proc. Natl. Acad. Sci. USA *117*, 7524–7535.

Belgareh-Touzé, N., Cavellini, L., and Cohen, M.M. (2017). Ubiquitination of ERMES components by the E3 ligase Rsp5 is involved in mitophagy. Autophagy *13*, 114–132.

Berger, K.H., Sogo, L.F., and Yaffe, M.P. (1997). Mdm12p, a component required for

mitochondrial inheritance that is conserved between budding and fission yeast. J. Cell Biol. *136*, 545–553.

Bleazard, W., McCaffery, J.M., King, E.J., Bale, S., Mozdy, A., Tieu, Q., Nunnari, J., and Shaw, J.M. (1999). The dynamin-related GTPase Dnm1 regulates mitochondrial fission in yeast. Nat. Cell Biol. *1*, 298–304.

Burgess, S.M., Delannoy, M., and Jensen, R.E. (1994). MMM1 encodes a mitochondrial outer membrane protein essential for establishing and maintaining the structure of yeast mitochondria. J. Cell Biol. *126*, 1375–1391.

Carman, G.M., and Han, G.S. (2011). Regulation of phospholipid synthesis in the yeast Saccharomyces cerevisiae. Annu. Rev. Biochem. *80*, 859–883.

Clancey, C.J., Chang, S.C., and Dowhan, W. (1993). Cloning of a gene (PSD1) encoding phosphatidylserine decarboxylase from Saccharomyces cerevisiae by complementation of an Escherichia coli mutant. J. Biol. Chem. *268*, 24580–24590.

Coffman, V.C., Wu, P., Parthun, M.R., and Wu, J.-Q. (2011). CENP-A exceeds microtubule attachment sites in centromere clusters of both budding and fission yeast. J. Cell Biol. *195*, 563–572.

Cox, J.S., Chapman, R.E., and Walter, P. (1997). The unfolded protein response coordinates the production of endoplasmic reticulum protein and endoplasmic reticulum membrane. Mol. Biol. Cell *8*, 1805–1814.

Dimmer, K.S., and Rapaport, D. (2017). Mitochondrial contact sites as platforms for phospholipid exchange. Biochim. Biophys. Acta Mol. Cell Biol. Lipids *1862*, 69–80.

Dimmer, K.S., Fritz, S., Fuchs, F., Messerschmitt, M., Weinbach, N., Neupert, W., and Westermann, B. (2002). Genetic basis of mitochondrial function and morphology in Saccharomyces cerevisiae. Mol. Biol. Cell *13*, 847–853.

Eisenberg-Bord, M., Shai, N., Schuldiner, M., and Bohnert, M. (2016). A tether is a tether is a tether: tethering at membrane contact sites. Dev. Cell *39*, 395–409.

Elbaz-Alon, Y., Rosenfeld-Gur, E., Shinder, V., Futerman, A.H., Geiger, T., and Schuldiner, M. (2014). A dynamic interface between vacuoles and mitochondria in yeast. Dev. Cell *30*, 95–102.

Friedman, J.R., Kannan, M., Toulmay, A., Jan, C.H., Weissman, J.S., Prinz, W.A., and Nunnari, J. (2018). Lipid homeostasis is maintained by dual targeting of the mitochondrial PE biosynthesis enzyme to the ER. Dev. Cell *44*, 261–270.e6.

Henry, S.A., Kohlwein, S.D., and Carman, G.M. (2012). Metabolism and regulation of glycerolipids in the yeast Saccharomyces cerevisiae. Genetics *190*, 317–349.

Hermann, G.J., Thatcher, J.W., Mills, J.P., Hales, K.G., Fuller, M.T., Nunnari, J., and Shaw, J.M. (1998). Mitochondrial fusion in yeast requires the transmembrane GTPase Fzo1p. J. Cell Biol. *143*, 359–373.

Hönscher, C., Mari, M., Auffarth, K., Bohnert, M., Griffith, J., Geerts, W., van der Laan, M., Cabrera, M., Reggiori, F., and Ungermann, C. (2014). Cellular metabolism regulates contact sites between vacuoles and mitochondria. Dev. Cell *30*, 86–94.

Jeong, H., Park, J., and Lee, C. (2016). Crystal structure of Mdm12 reveals the architecture and dynamic organization of the ERMES complex. EMBO Rep. *17*, 1857–1871.

Jeong, H., Park, J., Jun, Y., and Lee, C. (2017). Crystal structures of Mmm1 and Mdm12–Mmm1 reveal mechanistic insight into phospholipid trafficking at ER-mitochondria contact sites. Proc. Natl. Acad. Sci. USA *114*, E9502–E9511.

Joglekar, A.P., Bouck, D.C., Molk, J.N., Bloom, K.S., and Salmon, E.D. (2006). Molecular architecture of a kinetochore–microtubule attachment site. Nat. Cell Biol. *8*, 581–585.

Jumper, J., Evans, R., Pritzel, A., Green, T., Figurnov, M., Ronneberger, O., Tunyasuvunakool, K., Bates, R., Žídek, A., Potapenko, A., et al. (2021). Highly accurate protein structure prediction with AlphaFold. Nature *596*, 583–589.

Kakimoto, Y., Tashiro, S., Kojima, R., Morozumi, Y., Endo, T., and Tamura, Y. (2018). Visualizing multiple inter-organelle contact sites using the organelle-targeted split-GFP system. Sci. Rep. *8*, 6175.

Kawahara, T., Yanagi, H., Yura, T., and Mori, K. (1997). Endoplasmic reticulum stress-induced mRNA splicing permits synthesis of transcription factor Hac1p/Ern4p that activates the unfolded protein response. Mol. Biol. Cell *8*, 1845–1862.

Kawano, S., Tamura, Y., Kojima, R., Bala, S., Asai, E., Michel, A.H., Kornmann, B., Riezman, I., Riezman, H., Sakae, Y., et al. (2018). Structure–function insights into direct lipid transfer between membranes by Mmm1–Mdm12 of ERMES. J. Cell Biol. *217*, 959–974.

Kojima, R., Endo, T., and Tamura, Y. (2016). A phospholipid transfer function of ER-mitochondria encounter structure revealed in vitro. Sci. Rep. *6*, 30777.

Kojima, R., Kakimoto, Y., Furuta, S., Itoh, K., Sesaki, H., Endo, T., and Tamura, Y. (2019). Maintenance of cardiolipin and crista structure requires cooperative functions of mitochondrial dynamics and phospholipid transport. Cell Rep. *26*, 518–528.e6.

Korennykh, A.V., Egea, P.F., Korostelev, A.A., Finer-Moore, J., Zhang, C., Shokat, K.M., Stroud, R.M., and Walter, P. (2009). The unfolded protein response signals through high-order assembly of Ire1. Nature *457*, 687–693.

Kornmann, B., Currie, E., Collins, S.R., Schuldiner, M., Nunnari, J., Weissman, J.S., and Walter, P. (2009). An ER-mitochondria tethering complex revealed by a synthetic biology screen. Science *325*, 477–481.

Kornmann, B., Osman, C., and Walter, P. (2011). The conserved GTPase Gem1 regulates endoplasmic reticulum–mitochondria connections. Proc. Natl. Acad. Sci. USA *108*, 14151–14156.

Kurokawa, K., Ishii, M., Suda, Y., Ichihara, A., and Nakano, A. (2013). Live Cell Visualization of Golgi Membrane Dynamics by Super-resolution Confocal Live Imaging Microscopy (Elsevier Inc.).

Kurokawa, K., Okamoto, M., and Nakano, A. (2014). Contact of cis-Golgi with ER exit sites executes cargo capture and delivery from the ER. Nat. Commun. *5*, 3653.

Lang, A., John Peter, A.T., and Kornmann, B. (2015). ER–mitochondria contact sites in yeast: beyond the myths of ERMES. Curr. Opin. Cell Biol. *35*, 7–12.

Lawrimore, J., Bloom, K.S., and Salmon, E.D. (2011). Point centromeres contain more than a single centromere-specific Cse4 (CENP-A) nucleosome. J. Cell Biol. *195*, 573–582.

Longtine, M.S., Mckenzie, A., III, Demarini, D.J., Shah, N.G., Wach, A., Brachat, A., Philippsen, P., and Pringle, J.R. (1998). Additional modules for versatile and economical PCR-based gene deletion and modification in Saccharomyces cerevisiae. Yeast *14*, 953–961.

Meeusen, S., McCaffery, J.M., and Nunnari, J. (2004). Mitochondrial fusion intermediates revealed in vitro. Science *305*, 1747–1752.

Mozdy, A.D., McCaffery, J.M., and Shaw, J.M. (2000). Dnm1p GTPase-mediated mitochondrial fission is a multi-step process requiring the novel integral membrane component Fis1p. J. Cell Biol. *151*, 367–380.

Murley, A., and Nunnari, J. (2016). The emerging network of mitochondria-organelle contacts. Mol. Cell *61*, 648–653.

Nguyen, T.T., Lewandowska, A., Choi, J.-Y., Markgraf, D.F., Junker, M., Bilgin, M., Ejsing, C.S., Voelker, D.R., Rapoport, T.A., and Shaw, J.M. (2012). Gem1 and ERMES do not directly affect phosphatidylserine transport from ER to mitochondria or mitochondrial inheritance. Traffic *13*, 880–890.

Rasul, F., Zheng, F., Dong, F., He, J., Liu, L., Liu, W., Cheema, J.Y., Wei, W., and Fu, C. (2021). Emr1 regulates the number of foci of the endoplasmic reticulum-mitochondria encounter structure complex. Nat. Commun. *12*, 521–614.

Sam, P.N., Calzada, E., Acoba, M.G., Zhao, T., Watanabe, Y., Nejatfard, A., Trinidad, J.C., Shutt, T.E., Neal, S.E., and Claypool, S.M. (2021). Impaired phosphatidylethanolamine metabolism activates a reversible stress response that detects and resolves mutant mitochondrial precursors. iScience *24*, 102196.

Schneider, C.A., Rasband, W.S., and Eliceiri, K.W. (2012). NIH Image to ImageJ: 25 years of image analysis. Nat. Methods *9*, 671–675.

Schuck, S., Prinz, W.A., Thorn, K.S., Voss, C., and Walter, P. (2009). Membrane expansion alleviates endoplasmic reticulum stress independently of the unfolded protein response. J. Cell Biol. *187*, 525–536.

Sesaki, H., and Jensen, R.E. (1999). Division versus fusion: dnm1p and Fzo1p antagonistically regulate mitochondrial shape. J. Cell Biol. *147*, 699–706.

Sesaki, H., and Jensen, R.E. (2001). UGO1 encodes an outer membrane protein required for mitochondrial fusion. J. Cell Biol. *152*, 1123–1134.

Sesaki, H., Southard, S.M., Yaffe, M.P., and Jensen, R.E. (2003). Mgm1p, a dynamin-related GTPase, is essential for fusion of the mitochondrial outer membrane. Mol. Biol. Cell *14*, 2342–2356.

Sidrauski, C., and Walter, P. (1997). The transmembrane kinase Ire1p is a site-specific endonuclease that initiates mRNA splicing in the unfolded protein response. Cell *90*, 1031–1039.

Sikorski, R.S., and Hieter, P. (1989). A system of shuttle vectors and yeast host strains designed for efficient manipulation of DNA in Saccharomyces cerevisiae. Genetics *122*, 19–27.

Sogo, L.F., and Yaffe, M.P. (1994). Regulation of mitochondrial morphology and inheritance by Mdm10p, a protein of the mitochondrial outer membrane. J. Cell Biol. *126*, 1361–1373.

Sriburi, R., Jackowski, S., Mori, K., and Brewer, J.W. (2004). XBP1: a link between the unfolded protein response, lipid biosynthesis, and biogenesis of the endoplasmic reticulum. J. Cell Biol. *167*, 35–41.

Tamura, Y., and Endo, T. (2017). Role of intra- and inter-mitochondrial membrane contact sites in yeast phospholipid biogenesis. Adv. Exp. Med. Biol. *997*, 121–133.

Tamura, Y., Onguka, O., Hobbs, A.E.A., Jensen, R.E., Iijima, M., Claypool, S.M., and Sesaki, H. (2012). Role for two conserved intermembrane space proteins, Ups1p and Up2p, in intra-mitochondrial phospholipid trafficking. J. Biol. Chem. *287*, 15205–15218.

Tamura, Y., Kawano, S., and Endo, T. (2019a). Organelle contact zones as sites for lipid transfer. J. Biochem. *165*, 115–123.

Tamura, Y., Kojima, R., and Endo, T. (2019b). Advanced in vitro assay system to measure phosphatidylserine and phosphatidylethanolamine transport at ER/mitochondria interface. In Encyclopedia of Biophysics, pp. 57–67.

Tamura, Y., Kawano, S., and Endo, T. (2020). Lipid homeostasis in mitochondria. Biol. Chem. *401*, 821–833.

Tashiro, S., Kakimoto, Y., Shinmyo, M., Fujimoto, S., and Tamura, Y. (2020). Improved split-GFP systems for visualizing organelle contact sites in yeast and human cells. Front. Cell Dev. Biol. *8*, 571388–571417.

Tatsuta, T., and Langer, T. (2017). Intramitochondrial phospholipid trafficking. Biochim. Biophys. Acta Mol. Cell Biol. Lipids *1862*, 81–89.

Walter, P., and Ron, D. (2011). The unfolded protein response: from stress pathway to homeostatic regulation. Science *334*, 1081–1086.

Winston, F., Dollard, C., and Ricupero-Hovasse, S.L. (1995). Construction of a set of convenient Saccharomyces cerevisiae strains that are isogenic to S288C. Yeast *11*, 53–55.

Wong, E.D., Wagner, J.A., Gorsich, S.W., McCaffery, J.M., Shaw, J.M., and Nunnari, J. (2000). The dynamin-related GTPase, Mgm1p, is an intermembrane space protein required for maintenance of fusion competent mitochondria. J. Cell Biol. *151*, 341–352.

Yamamoto, H., Kakuta, S., Watanabe, T.M., Kitamura, A., Sekito, T., Kondo-Kakuta, C., Ichikawa, R., Kinjo, M., and Ohsumi, Y. (2012). Atg9 vesicles are an important membrane source during early steps of autophagosome formation. J. Cell Biol. *198*, 219–233.

STAR★METHODS

KEY RESOURCES TABLE

REAGENT or RESOURCE	SOURCE	IDENTIFIER
Antibodies		
Rabibit polyclonal anti-Mmm1	Endo Lab	N/A
Rabibit polyclonal anti-Mdm34	Endo Lab	N/A
Rabibit polyclonal anti-Mdm12	Endo Lab	N/A
Rabibit polyclonal anti-Tim23	Endo Lab	N/A
Rabibit polyclonal anti-Porin	Endo Lab	N/A
Rabibit polyclonal anti-Fzo1	Endo Lab	N/A
Rabibit polyclonal anti-Mgm1	Tamura Lab	N/A
Rabibit polyclonal anti-Ugo1	Sesaki Lab	N/A
Rabibit polyclonal anti-Dnm1	Endo Lab	N/A
Rabibit polyclonal anti-Tom70	Endo Lab	N/A
Rabibit polyclonal anti-Opi3	Tamura Lab	N/A
Rabibit polyclonal anti-Kar2	Endo Lab	N/A
Rabibit polyclonal anti-Pdi	GENETEX, Inc.	Cat# GTX50319; RRID:AB_625705
mouse monoclonal anti-GFP	Takara Bio	Cat# 632380; RRID:AB_10013427
Cy5 AffiniPure Goat Anti-Rabbit IgG (H+L)	Jackson ImmunoResearch Labs	Cat# 111-175-144; RRID:AB_2338013
Goat anti-Rabbit IgG (H+L) Cross-Adsorbed Secondary Antibody, HRP	Thermo Fisher Scientific	Cat# A16104, RRID:AB_2534776)
Goat anti-Mouse IgG (H+L) Cross-Adsorbed Secondary Antibody, HRP	Thermo Fisher Scientific	Cat# A16072; RRID:AB_2534745
Bacterial and virus strains		
XL2-blue	N/A	N/A
Chemicals, peptides, and recombinant proteins		
Tunicamycin	Nakalai tesque	Cat# 35638-74
DTT	FUJIFILM Wako Pure Chemical	Cat# M02712
PVDF membrane (Immobilon-P)	Merck-Millipore	Cat# IPVH00010
PVDF membrane (Immobilon-FL)	Merck-Millipore	Cat# PFL00010
Experimental Models: Organisms/Strains		
All listed below are *Saccharomyces cerevisiae* strains		
FY833- MATa *ura3-52 his3-Δ200 leu2-Δ1 lys2-Δ202 trp1-Δ63*	Winston et al. (1995)	N/A
FY834- MATα *ura3-52 his3-Δ200 leu2-Δ1 lys2-Δ202 trp1-Δ63*	Winston et al. (1995)	N/A
rho^0- MATa *ura3-52 his3-Δ200 leu2-Δ1 lys2-Δ202 trp1-Δ63 rho^0*	This study	N/A
fzo1Δ- MATa *ura3-52 his3-Δ200 leu2-Δ1 lys2-Δ202 trp1-Δ63 fzo1Δ::kanMX4 rho^0*	This study	N/A
Mmm1-GFP- MATa *ura3-52 his3-Δ200 leu2-Δ1 lys2-Δ202 trp1-Δ63 MMM1-GFP::TRP1*	Tamura et al. (2012)	N/A

(*Continued on next page*)

Continued

REAGENT or RESOURCE	SOURCE	IDENTIFIER
Mmm1-GFP dnm1Δ- MATa *ura3-52 his3-Δ200 leu2-Δ1 lys2-Δ202 trp1-Δ63 MMM1-GFP::TRP1 dnm1Δ::URA3*	This study	N/A
Mmm1-GFP vps39Δ- MATa *ura3-52 his3-Δ200 leu2-Δ1 lys2-Δ202 trp1-Δ63 MMM1-GFP::TRP1 vps39Δ::hphMX*	This study	N/A
Mmm1-GFP ypt7Δ- MATa *ura3-52 his3-Δ200 leu2-Δ1 lys2-Δ202 trp1-Δ63 MMM1-GFP::TRP1 ypt7Δ::hphMX*	This study	N/A
Mmm1-GFP rho^0- MATa *ura3-52 his3-Δ200 leu2-Δ1 lys2-Δ202 trp1-Δ63 MMM1-GFP::TRP1 rho^0*	This study	N/A
Mmm1-GFP fzo1Δ- MATa *ura3-52 his3-Δ200 leu2-Δ1 lys2-Δ202 trp1-Δ63 MMM1-GFP::TRP1 fzo1Δ::kanMX4 rho^0*	This study	N/A
Mmm1-GFP fzo1Δdnm1Δ- MATa *ura3-52 his3-Δ200 leu2-Δ1 lys2-Δ202 trp1-Δ63 MMM1-GFP::TRP1 fzo1Δ::kanMX4 dnm1Δ:: kanMX4*	This study	N/A
Mmm1-GFP ugo1Δ- MATa *ura3-52 his3-Δ200 leu2-Δ1 lys2-Δ202 trp1-Δ63 MMM1-GFP::TRP1 ugo1Δ::HIS3 rho^0*	This study	N/A
Mmm1-GFP ugo1Δdnm1Δ- MATa *ura3-52 his3-Δ200 leu2-Δ1 lys2-Δ202 trp1-Δ63 MMM1-GFP::TRP1 ugo1Δ::HIS3 dnm1Δ:: kanMX4*	This study	N/A
Mmm1-GFP mgm1Δ- MATa *ura3-52 his3-Δ200 leu2-Δ1 lys2-Δ202 trp1-Δ63 MMM1-GFP::TRP1 mgm1Δ::kanMX4 rho^0*	This study	N/A
Mmm1-GFP mgm1Δdnm1Δ- MATa *ura3-52 his3-Δ200 leu2-Δ1 lys2-Δ202 trp1-Δ63 MMM1-GFP::TRP1 mgm1Δ::kanMX4 dnm1Δ::kanMX4*	This study	N/A
Mmm1-GFP ire1Δ- MATa *ura3-52 his3-Δ200 leu2-Δ1 lys2-Δ202 trp1-Δ63 MMM1-GFP::TRP1 ire1Δ::kanMX4*	This study	N/A
Mmm1-GFP hac1Δ- MATa *ura3-52 his3-Δ200 leu2-Δ1 lys2-Δ202 trp1-Δ63 MMM1-GFP::TRP1 hac1Δ::kanMX4*	This study	N/A
Mmm1-GFP ino2Δ- MATa *ura3-52 his3-Δ200 leu2-Δ1 lys2-Δ202 trp1-Δ63 MMM1-GFP::TRP1 ino2Δ::kanMX4*	This study	N/A
Mmm1-GFP ino4Δ- MATa *ura3-52 his3-Δ200 leu2-Δ1 lys2-Δ202 trp1-Δ63 MMM1-GFP::TRP1 ino4Δ::kanMX4*	This study	N/A
Mmm1-GFP gem1Δ- MATa *ura3-52 his3-Δ200 leu2-Δ1 lys2-Δ202 trp1-Δ63 MMM1-GFP::TRP1 gem1Δ::kanMX4*	This study	N/A
Mmm1-GFP mco6Δ- MATa *ura3-52 his3-Δ200 leu2-Δ1 lys2-Δ202 trp1-Δ63 MMM1-GFP::TRP1 mco6Δ::kanMX4*	This study	N/A

(*Continued on next page*)

Continued

REAGENT or RESOURCE	SOURCE	IDENTIFIER
GAL-Mmm1-GFP- MATa *ura3-52 his3-Δ200 leu2-Δ1 lys2-Δ202 trp1-Δ63 His3MX6-GAL1-MMM1-GFP::TRP1*	This study	N/A
GAL-Mmm1-mScarlet- MATα *ura3-52 his3-Δ200 leu2-Δ1 lys2-Δ202 trp1-Δ63 His3MX6-GAL1-MMM1-mScarlet::kanMX4*	This study	N/A
Mmm1-GFP Idh1-mCherry- MATa *ura3-52 his3-Δ200 leu2-Δ1 lys2-Δ202 trp1-Δ63 MMM1-GFP::TRP1 IDH1-mCherry::kanMX6*	This study	N/A
Mmm1-3PA-GFP- MATa *ura3-52 his3-Δ200 leu2-Δ1 lys2-Δ202 trp1-Δ63 MMM1-3PA-GFP::TRP1*	This study	N/A
Cse4-GFP- MATa *ura3-52 his3-Δ200 leu2-Δ1 lys2-Δ202 trp1-Δ63 Cse4-GFP::TRP1*	This study	N/A
YPH250-*MATa ura3-52 lys2-801 ade2-101 trp1-Δ1 his3-Δ200 leu2-Δ1 gal3*	Sikorski and Hieter, 1989	N/A
mmm1-1- MATa *ura3-52 lys2-801 ade2-101 trp1-Δ1 his3-Δ200 leu2-Δ1 gal3 mmm1-1*	Burgess et al. (1994)	N/A
Mdm12-GFP- MATa *ura3-52 lys2-801 ade2-101 trp1-Δ1 his3-Δ200 leu2-Δ1 gal3 MDM12-GFP::TRP1*	This study	N/A
Mdm12-GFP/mmm1-1- MATa *ura3-52 lys2-801 ade2-101 trp1-Δ1 his3-Δ200 leu2-Δ1 gal3 MDM12-GFP::TRP1 mmm1-1*	This study	N/A
psd2Δdpl1Δ- MATa *ura3-52 his3-Δ200 leu2-Δ1 lys2-Δ202 trp1-Δ63 psd2Δ::HIS3 dpl1Δ::URA3*	This study	N/A
psd2Δdpl1Δrho^0- MATa *ura3-52 his3-Δ200 leu2-Δ1 lys2-Δ202 trp1-Δ63 psd2Δ::HIS3 dpl1Δ::URA3 rho^0*	This study	N/A
psd2Δdpl1Δfzo1Δ- MATa *ura3-52 his3-Δ200 leu2-Δ1 lys2-Δ202 trp1-Δ63 psd2Δ::HIS3 dpl1Δ::URA3 fzo1Δ::TRP1 rho^0*	This study	N/A
Oligonucleotides		
AACATTATCTGATATCACGGAT AGAGGCAAAACGGTAGGCTCAT TTAACGGTTGTAAAACGACGGCCAGT	This study	YU29
TAACATTATGTATATTGATTTGAAA AGACCTCATATATTTACAAGAATAT CACAGGAAACAGCTATGACC	This study	YU30
TCTCTGCCGATTTTTGGTTTCCAA TAGTATAGGTTTAACTCAACCCCC CAGTTGTAAAACGACGGCCAGT	This study	YU31
CACTGGAATACCATGGGCGAACAT AAAAAAAAATGGGGGACTATCCCA GTCACAGGAAACAGCTATGACC	This study	YU32
TTTCGTACTTATAATATAGCCTCG CATATTCACCATAATACTCTGAAA GCGTTGTAAAACGACGGCCAGT	This study	YU33

(*Continued on next page*)

Continued

REAGENT or RESOURCE	SOURCE	IDENTIFIER
CGGTAAAAAATGCTATTTACAAAT TCTCTAATGACACTATTTATTTTAC ACACAGGAAACAGCTATGACC	This study	YU34
GACGGGTCTTATATTGATCAGCA AAAACCCTTCAAAATATCAATTTA TACCAAAAATTAAGTTGTAAAAC GACGGCCAGT	This study	NU831
GAGAGATTTTTAATATATATAAG AAATACTAACAACAATAACAGC AGCTGTTAAGGGATCCACAGG AAACAGCTATGACC	This study	NU832
GTTACCAAGTATGTGGCCACGTAG TAAAAATACGAGAGAAGAAAAGCC TACAGAGTTACGGATCCCCGGGTTAATTAA	This study	NU1174
CCAAAAATGAGGCAGAGAAGA TAGGAAAAAGATAGAACAAAAAA TTTGTACATAAATATGAATTCGAGCT CGTTTAAAC	This study	NU1175
TGAAAGAACTTTGAGAGAGTCAA TATAATACCTGTAGCCTTTTTCTGA AAGAATTCGAGCTCGTTTAAAC	This study	YU1071
CAAACGTCATTAACGAATCCGT TTCGGTGGATTCATTCTCACTATC AGTCATTTTGAGATCCGGGTTTT	This study	YU1072
CATAGAAGCACAGATCAGAGCA CAGCCATACAACATAAGTGTTGT AAAACGACGGCCAGT	This study	YU1116
TCTTATGTATGTACGTATGTGCTGA TTTTTTATGTGCTTGCACAGGAAACA GCTATGACC	This study	YU1117
CCTCTTCCCCACGTCCATTATCAC	This study	YU1347
GTATGTCGATGTTCGATGTTTATGAG	This study	YU1348
GTTCTCTTTTGTTCTCGCTCCCTACATTC	This study	YU1349
ATTGTAGGAGGGCGCGCCAACCTCACG	This study	YU1350
CAAGAACCTTCAAATAACTGGAAA TGGGGCATGGAGGATAGCGCCGC AGCTTATCATCGGATCCCCGGGTTAATTAA	This study	YU1518
ATCGGAGAGTATGTATTTGTGTAGT TATGTACTTAGATATGTAACTTAATGA ATTCGAGCTCGTTTAAAC	This study	YU1519
TAATGAAGAAAGACATGCAACTAG CAAGAAGAATCAGGGGACAGTTTA TTCGGATCCCCGGGTTAATTAA	This study	YU1563
AAACCCCGAAAAAGGGAAAAATCG GCTCCAGCCCTGAAGCACAAATAT CAGAATTCGAGCTCGTTTAAAC	This study	YU1564
Recombinant DNA		
pBS-*kanMX4*	Endo Lab	N/A
pBS-*hphMX*	Endo Lab	N/A
pFA6a-GFP(S65T)-TRP1	Longtine et al. (1998)	N/A

(*Continued on next page*)

Continued

REAGENT or RESOURCE	SOURCE	IDENTIFIER
pFA6a-His3MX6-PGAL1	Longtine et al. (1998)	N/A
pFA6a-mScarlet-kanMX4	Kakimoto et al. (2018)	N/A
pRS316-su9-RFP	Kakimoto et al. (2018)	N/A
pRS315-Su9-RFP	Kakimoto et al. (2018)	N/A
pRS315-Su9-BFP	Tashiro et al. (2020)	N/A
pRS316-Tom71-mCherry	Kakimoto et al. (2018)	N/A
pRS315-BipN-GFP-HDEL	Kakimoto et al. (2018)	N/A
pRS424-Psd1	Kojima et al., 2019	N/A
pRS314-Mmm1-GFP	This study	N/A
pRS314-Mmm1ΔN1-GFP	This study	N/A
pRS314-Mmm1ΔN2-GFP	This study	N/A
pRS314-Mmm1ΔN3-GFP	This study	N/A
pRS314-Mmm1ΔN4-GFP	This study	N/A
pRS314-Mmm1ΔN5-GFP	This study	N/A
pRS314-Mmm1ΔN6-GFP	This study	N/A
Software		
ImageJ	Schneider et al., 2012	https://imagej.nih.gov/ij/
GraphPad Prism6	GraphPad	https://www.graphpad.com/scientific-software/prism/

RESOURCE AVAILABILITY

Lead contact

Further information and requests for resources and reagents should be directed to and will be fulfilled by the lead contact, Yasushi Tamura (tamura@sci.kj.yamahgata-u.ac.jp).

Materials availability

Plasmids and yeast strains generated in this study are available from the lead contact.

Data and code availability

All data reported in this article will be shared by the lead contact upon request.

This paper does not report original code.

Any additional information required to reanalyze the data reported in this paper is available from the lead contact upon request.

EXPERIMENTAL MODEL AND SUBJECT DETAILS

In this study, we used a *Saccharomyces cerevisiae* strain, FY833 (MATa *ura3-52 his3-Δ200 leu2-Δ1 lys2-Δ202 trp1-Δ63*) or FY834 (MATα *ura3-52 his3-Δ200 leu2-Δ1 lys2-Δ202 trp1-Δ63*) as background strains (Winston et al., 1995). All the yeast cells used in this study are listed in the key resources table.

METHOD DETAILS

Strains, plasmids, primers, and growth conditions

Saccharomyces cerevisiae strain FY833 (MATa *ura3-52 his3-Δ200 leu2-Δ1 lys2-Δ202 trp1-Δ63*) and FY834 (MATα *ura3-52 his3-Δ200 leu2-Δ1 lys2-Δ202 trp1-Δ63*) were used as background strains (Winston et al., 1995). The yeast cells used in this study are listed in Table S1. Yeast KO and DAMP strains used in this study are following; KO strains: *ayr4*, *bna4*Δ, *cbr1*Δ, *eht1*Δ, *erg6*Δ, *faa1*Δ, *fis1*Δ, *fzo1*Δ, *gem1*Δ, *gsf2*Δ, *gtt1*Δ, *hfd1*Δ, *lsp1*Δ, *mcr1*Δ, *mdm10*Δ, *mdm34*Δ, *mdv1*Δ, *mmm1*Δ, *mmr1*Δ, *msp1*Δ, *om45*Δ, *pdh1*Δ, *pil1*Δ,

*por2*Δ, *pth2*Δ, *rd11Δ*, *sac1*Δ, *ste24*Δ, *tcd1*Δ, *tcd2*Δ, *tom6*Δ, *ubp16*Δ, *ubx2*Δ, *ugo1*Δ, *uip4*Δ, *vps1*Δ, *vps21*Δ, *yju3*Δ, *ypt31*Δ, *ypt32*Δ, *ypt7*Δ; DAmP Yeast strains: *dpm1*, *ncp1*, *sam35*, *sam37*, *sec4*, *sen2*, *sen34*, *sen54*, *tom22*, *tom40*, *tsc10*. Yeast cells expressing Mmm1-GFP originating from FY833 was used as the wild-type strain (Tamura et al., 2012). The C-terminal GFP or mScarlet tagging, introduction of the *GAL1* promoter in front of the *MMM1* or *CHO1* gene, and gene disruptions were performed by homologous recombination using the appropriate gene cassettes amplified from the plasmids listed in Table S2 (Kojima et al., 2019; Longtine et al., 1998). The primer pairs #YU1116/1117, #YU29/30, #YU31/32, #YU1347/1348, and #YU1349/1350 were used to amplify the gene cassette for the disruption of *FIS1*, *FZO1*, *UGO1*, *IRE1*, and *HAC1* gene, respectively. To introduce the GFP or mScarlet tag for *MMM1*, *CSE4,* and the *GAL1* promoter for *MMM1* and *CHO1*, the appropriate gene cassettes were respectively amplified with the primer pair #NU1174/1175, #YU1563/1564, #YU2047/2048, #YU1071/1072, or #YU2514/2515. All the primer sequences were indicated in Table S2.

Yeast cells were grown in YPD (1% yeast extract, 2% polypeptone, and 2% glucose), SCD (0.67% yeast nitrogen base without amino acids, 0.5% casamino acid, and 2% glucose), SD (0.67% yeast nitrogen base without amino acids, 0.13% drop-out amino acid mix and 2% glucose) media with appropriate supplements. The drop-out amino acid mix was a mixture of 2.6 g adenine, 6.0 g L-aspartic acid, 12 g L-threonine, 2.6 g L-asparagine, 1.8 g L-tyrosine, 6.0 g L-glutamic acid, 2.6 g L-glutamine, 2.6 g glycine, 2.6 g L-alanine, 2.6 g L-isoleucine, 1.2 g L-methionine, 3.0 g L-phenylalanine, 2.6 g L-proline, 22.6 g L-serine, 9.0 g L-valine and 2.6 g L-cysteine (all amounts are per liter).

Fluorescence microscopy

Logarithmically growing yeast cells cultivated in SCD or SD media were observed using a model IX83 microscope (Olympus) with a CSU-X1 confocal unit (Yokogawa), a 100× and 1.4 numerical aperture objective lens (UPlanSApo; Olympus), and an sCMOS camera (Zyla 5.5; Andor). Image analysis involved MetaMorph software (Molecular Devices). To observe mScarlet signal, we used an Evolve 512 EM-CCD camera (Photometrics). GFP or RFP/mScarlet were excited using a 488-nm or 561-nm laser (OBIS; Coherent) and the emission was passed through 520/35-nm or 617/73-nm band-pass filter, respectively. The confocal fluorescent sections were collected every 0.2 μm from the upper to the bottom surface of yeast cells. The obtained confocal images were subjected to maximum projection using Image J software (NIH). To enumerate ERMES dots, Mmm1-GFP dots were automatically picked by the TransFluor macro for MetaMorph software using the "Pits" algorithm. The resulting images containing the selected dots were counted. Signal intensities of ERMES and Cse4-GFP dots were calculated using Image J software.

SCLIM was developed by the combined use of the model IX-71 inverted fluorescence microscope with a UPlanSApo 100 X NA 1.4 oil objective lens (Olympus), a high-speed and high-signal-to noise-ratio spinning-disk confocal scanner (Yokogawa Electric), a custom-made spectroscopic unit, image intensifiers (Hamamatsu Photonics) equipped with a custom-made cooling system, magnification lens system to provide 266.7× final magnification, and three EM-CCD cameras (Hamamatsu Photonics) for green, red, and infrared observation (Kurokawa et al., 2013). Images were acquired using custom-made software (Yokogawa Electric). For three-dimensional (3D) time-lapse imaging, we collected optical sections spaced 0.2 μm apart in stacks by oscillating the objective lens vertically with a custom-made piezo actuator. Z-stack images were converted to 3D voxel data and processed by deconvolution with Volocity (Perkin Elmer) using the theoretical point-spread function for spinning-disk confocal microscopy.

Immunoblotting and antibodies

For immunoblotting, proteins were transferred to polyvinylidene fluoride Immobilon-FL or Immobilon-P membranes (Millipore). The transferred proteins were detected by fluorophore- or horseradish peroxidase (HRP)-conjugated to secondary antibodies (Cy5 AffiniPure Goat Anti-Rabbit IgG (H+L), Jackson ImmunoResearch Laboratories) or goat anti-Rabbit IgG (H+L) cross-adsorbed secondary antibody conjugated to HRP (Thermo Fisher Scientific) and analyzed with a Typhoon imager (GE Healthcare) or LAS-4000 mini device (Fujifilm).

In vivo pulse-chase experiment with ^{14}C serine

The pulse-chase experiments were performed essentially as described previously (Tamura et al., 2012). Specifically, *psd2Δdpl1Δ* cells were first cultivated to logarithmic phase in 5 mL of YPD medium and sedimented by centrifugation. The collected cells were suspended in 1 mL of PBS containing 3 μCi/mL

^{14}C-serine for 15 min at 30°C unless otherwise stated. After the pulse-labeling, the cells were washed with YPD medium and suspended in 5.5 mL of the same medium. Then, 1 mL of the cell suspension was immediately collected as the zero time-point sample. The cells collected by centrifugation were resuspended in 330 μL methanol and kept on ice until all pulse-chase samples were prepared. The rest of the cells were sampled at predetermined times, collected by centrifugation, and resuspended in 330 μL of methanol after the chase cultivation. We added 100 μL of glass beads to the samples and vortexed for 15 min. Subsequently, we added 660 μL of chloroform to the samples, centrifuged them at 12,000 ×*g* for 10 min, and transfer the supernatant to new tubes. The samples were added with 200 μL of 0.1 M HCl/0.1M KCl and vortexed for 5 min. The organic phase was separated by centrifugation at 400 × *g* for 5 min, dried under N_2 gas, and resuspended in chloroform. All the samples were analyzed by thin-layer chromatography (TLC) followed by radioimaging.

In vitro phospholipid transport assay with ^{14}C serine

The *in vitro* assays were performed essentially as described previously (Kojima et al., 2016; Tamura et al., 2019b). Specifically, we isolated heavy membrane fractions (12,000 × *g* pellet) from yeast cells cultured in SCD media. The isolated membrane fractions were incubated at 30°C for a period of time. in assay buffer (300 mM sucrose, 20 mM Tris-HCl, pH 7.5, 40 mM KCl, 2 mM CTP, 1 mM S-adenosylmethionine, 0.1 mM $MnCl_2$, 2 mM $MgCl_2$) in the presence of 2 μ Ci/mL[^{14}C(U)]-L-serine. To stop PS synthesis and its transport reactions, we added 900 μ L of 2:1 chloroform/methanol to 100 μ of the samples and vortexing for 15 min. Then, 200 μ L of 0.1M KCl, 0.1 M HCl was added to the samples and further vortexed for 15 min at room temperature. After 5 min spin, the organic phase was collected and dried under N_2 gas. The resulting lipids were dissolved in chloroform and subjected to the analysis by TLC followed by radioimaging with an Amersham Typhoon scanner.

QUANTIFICATION AND STATISTICAL ANALYSIS

The number of ERMES per cell and signal intensities of ERMES and Cse4-GFP dots are shown as box and whisker plots (Tukey). The sample number is indicated in the figure legends. Data are shown as mean with standard error of the mean or standard deviation as indicated in the figure legends. Student's t-test with Welch's correction were performed for the statistical analyses using Prism 6 software (GraphPad).